Renewable and Sustainable Energy Reviews 70 (2017) 193–214

Contents lists available at ScienceDirect

Renewable and Sustainable Energy Reviews

journal homepage: www.elsevier.com/locate/rser

Renewable energy harvesting by vortex-induced motions: Review and benchmarking of technologies

Ali Bakhshandeh Rostami*, Mohammadmehdi Armandei

Department of Ocean Engineering, Universidade Federal do Rio de Janeiro (UFRJ), Rio de Janeiro, Brazil

ARTICLE INFO

Keywords:
Vortex-induced motions
Flutter
Galloping
Buffeting
Vortex-Induced Vibration (VIV)
Fluttering-Autorotation
Renewable energy harvesting
Benchmarking

ABSTRACT

Vortex-induced motions are generally known as destructive phenomena for engineering structures. Nevertheless, they have a positive effect which is their great potential to extract renewable energy from the fluid flow. The phenomenology of vortex-induced motions has been studied and several energy harvesting technologies based on these motions have been reported, separately through literature. However, a comprehensive study that bonds together the phenomenology and the energy extraction technologies does not exist yet. Now that this area has become well established, classification of the relevant phenomena and technologies has become necessary as well. The present paper has two main objectives; The first objective is to classify the whole vortex-induced motion phenomena into several groups which include Flutter, Transverse and Torsional Galloping, Buffeting, Vortex-Induced Vibration (VIV), and Fluttering-Autorotation. The second objective is to review the literature, with the aim of classifying different technologies of renewable energy harvesting based on vortex-induced motion. Also, the performance characteristics and economical costs of these technologies are benchmarked.

1. Introduction and background

From long time ago, human society have used the energy of wind and current to do several activities, such as mill grains and pump waters in the past and generate electricity recently. Traditionally, turbines and watermills have been in use for extracting energy from these resources. Examples of these devices are the reaction turbines such as Francis turbine, impulse turbines such as Pelton wheels, or impulse and reaction turbines such as modern wind turbines. These devices have relatively high efficiency; however there are some remarkable disadvantages in regard to use of these devices.

One of the disadvantages about the traditional turbines and watermills is their requirement to high energy fluid flow for working. For instance, in hydropower turbine, high hydraulic head is needed for running the turbine. Although the hydraulic head can occur naturally, e.g. waterfall, it is not always the case. In most cases, high hydraulic head is created by constructing a dam on a river. The cost of dam construction makes traditional hydroelectric projects difficult to execute. In spite of the cost, building a dam will increase safety risks, such as flash flood caused by a broken dam, and environmental and ecological complications such as silt accumulation in basin.

Other disadvantage, mostly attended to impulse and reaction turbines, is due to their particular design. The inborn structural weakness associated with centrifugal stress necessitates high performance materials and thus the construction costs are increased. Moreover, in conventional designs, e.g. the horizontal axis wind turbines, large translational speed is reached at the tips of the blades. In large wind turbines, this speed approaches the sound barrier causing serious environmental concerns about noise generation as well as the threat they pose to birds [1].

Recently, a new paradigm to extract energy from wind and current has been developed which is based on vortex-induced motions. In this paradigm, the energy of vortices is recovered instead of providing flow with extra energy artificially. A vortex is a rotating region in fluid medium that can be simplified by many concentric circular layers which rotate in different angular velocity [2]. Vortex shedding, due to which vortices are generated and detached from the body, changes the local pressure distribution around the body [12]. This local change in pressure distribution induces motion on the body. Vortex generation repeats periodically and therefore, the body moves continuously.

In the recent decades, a lot of studies have been performed to develop the knowledge and new technologies have been introduced in the field of energy extraction from vortex-induced motion. However, a comprehensive classification to categorize the relevant phenomena and technologies does not exists yet. The objectives of this work are; (1) to classify the whole vortex-induced motion phenomena into several

* Corresponding author.
E-mail address: rostami115@gmail.com (A.B. Rostami).

http://dx.doi.org/10.1016/j.rser.2016.11.202
Received 13 June 2016; Received in revised form 29 September 2016; Accepted 14 November 2016

groups, and (2) to review the energy extraction technologies related to each class. Also, the technologies are benchmarked by different criteria. The classification and the phenomena description of vortex-induced motion are presented in Section 2. The literature about the energy extraction using the described phenomena is reviewed in Section 3. Section 4 gives the performance and the energy cost benchmarking of the vortex-induced motion phenomena. Also, the cost of vortex-induced motion energy harvesting technologies is compared to other traditional and alternative energy resources. Finally, the conclusion is presented in Section 5.

2. Vortex-induced motions (VIM): classification

Vortex-induced motions (VIM) place into two main groups of oscillation type and rotation type. Oscillation types are classified in two general categories; instability type and resonance type [4,5]. In instability type the forces vary with time as a result of the motion of the structure, and increase the oscillation amplitude. The instability is called Flutter when the resulting oscillation is in two or more coupled degrees of freedom, and Galloping when the oscillation has only one degree of freedom. Galloping, in its turn, has two types; transverse and torsional. On the other hand, in resonance type, the elastic structure begins to oscillate if the frequency of the oscillatory forces corresponds to its natural frequency. The oscillatory force can be either by the oscillating incoming flow, i.e. Buffeting, or induced due to the vortex shedding, i.e. Vortex-Induced Vibration (VIV) and Fluttering.[1] As the inertia increases, Fluttering which is an oscillatory rotation is converted to Autorotation which is continuous rotation. In other words, there is a bifurcation between Fluttering and Autorotation, i.e. rotation type VIMs. A flowchart of flow-induced oscillations is shown in Fig. 1. The phenomenology of VIMs is briefly introduced in the following sections.

2.1. Flutter

Flutter is a self-controlled oscillation due to hydro/aero elastic instability, and usually applies for two degree of freedom aeroelastic oscillation of aircraft wings [6]. A simplified two-dimensional representation of an airfoil is shown in Fig. 2 where the foil is restrained elastically in torsion and vertical bending. The aerodynamic lift forces classically places in one-quarter of the chord aft of the foil leading edge, so-called “Aerodynamic center” [7]. In this figure, the connection point of elastic axis is at the center of rotation. Hydro/aero elastic instability happens when the center of gravity places aft of the center of rotation. On the contrary, the stable condition comes from putting the center of gravity forward of the center of rotation.

In flutter, there is an inertial coupling between the two degrees of freedom [8]. The phase difference is an essential part of the instability in flutter. In this process the two independent translational and torsional frequencies are driven together by aerodynamic stiffness terms. This coupled motion initiates when the encountered flow reaches to special velocity. This velocity is known as cut-in velocity or flutter boundary velocity.

Singh et al. [9] have justified the cut-in speed as the responsible part of the fluid for flutter instability. They have reported that the oscillation happens for a certain range of current speeds regardless to geometry. The interesting point which was reported in their work is that the inviscid part of the fluid is responsible for instability because the inviscid forces cause to finite amplitude oscillations. Also, they have stated that the viscous part of the flow only extends the range of speed corresponding instability without any changes on the fundamental physics of flutter oscillations. Fei and Li [10] have given an empirical equation for critical flutter speed (cut-in velocity), which can be written as:

$$U_C = \frac{1.76}{B}\, r \sqrt{\frac{m}{\pi\rho}(\omega_P^2 - \omega_H^2)} \tag{1}$$

where r is radius of gyration of the cross-section ($I=mr^2$); m is the mass per unit length; B is the structure width; ρ is the flow density; ω_P and ω_H are the angular frequencies in rotational direction (pitch motion) and translational direction (heave), respectively.

By observing nonlinear bifurcations, aeroelastic responses can be determined in the vicinity of the flutter boundary. This nonlinear analysis can determine the LCO stability. In Fig. 3a general bifurcation plot depicts two different LCO responses [11]. It can be clearly seen that when weak nonlinearities are present in the aero/hydro elastic system the LCO quickly reaches large amplitude with a consequent divergent behavior. Conversely, strong nonlinearities create a more stable LCO response.

Flutter includes various types such as torsion-plunge coupled instability (flutter), unstable torsion (divergence), and single degree of freedom oscillation (stall flutter)[14].

2.2. Galloping

Suppose an elastic body stirs up when placed in fluid flow. The fluid forces, generated by relative motion of the body and fluid, cause that the oscillation amplitude descends and body remains stable, or ascends and motion becomes unstable. Therefore, the stability or instability of the body depends on the ratio between the transmitting energy to vibrating body due to the forces and the dissipated energy from the system that is named energy ratio. Hence, the body becomes unstable if the energy ratio is greater than 1 and in the contrary, becomes stable if the ratio of energy being less than 1.

Galloping is known as dynamic instability that is induced in an elastic structure due to internal turbulence of the fluid or any other reason which provides initial disturbance. Therefore, galloping enhances any initial small motion of the structure and turns it to an oscillation. The oscillation occurs in a plane normal to the oncoming flow velocity. Some references define it as a velocity-dependent, damping-controlled instability, which unlike Flutter is a one degree-of-freedom [13,4,14]. This instability gives rise to Transverse (translational) galloping or torsional galloping and has relatively high amplitude.

2.2.1. Transverse galloping

Consider a prismatic body connected to a linear spring, subjected to an incoming flow in the transverse direction, with a mass per unit length m, mechanical damping ratio ζ, and natural circular frequency of oscillation ω_n (see Fig. 4). The only degree-of-freedom of such structure is transverse oscillation. Moreover, the body is sufficiently slender to consider bi-dimensional flow, and the incident flow is free of turbulence. Then, the equation governing the dynamics of the system is

$$m(\ddot{y}+2\zeta\omega_n\dot{y} + \omega_n{}^2 y) = F_y = \frac{1}{2}\rho U^2 D C_y \tag{2}$$

where y denotes the vertical position, ρ is the fluid density, U is the undisturbed velocity of the incident flow, D is the characteristic dimension of the body normal to the flow, F_y is the fluid force per unit length in the normal direction to the incident flow, C_y is the instantaneous fluid force coefficient also in the transverse direction to the incident flow, and the dot symbol stands for differentiation with respect to time t. Fig. 4 implies that

$$F_y = -F_D \sin\alpha - F_L \cos\alpha \tag{3}$$

Any increase in the vertical velocity of the body ($\Delta\dot{y}>0$) will result in $\Delta\alpha > 0$. Besides, the system would be stable if $dF_y/d\alpha<0$, because $\Delta\dot{y}>0$ and $dF_y<0$, and hence the transverse oscillation will decay. On the other hand, for $dF_y/d\alpha>0$ the transverse oscillation will grow and lead to

[1] Note that there is difference between *flutter* and *fluttering*.

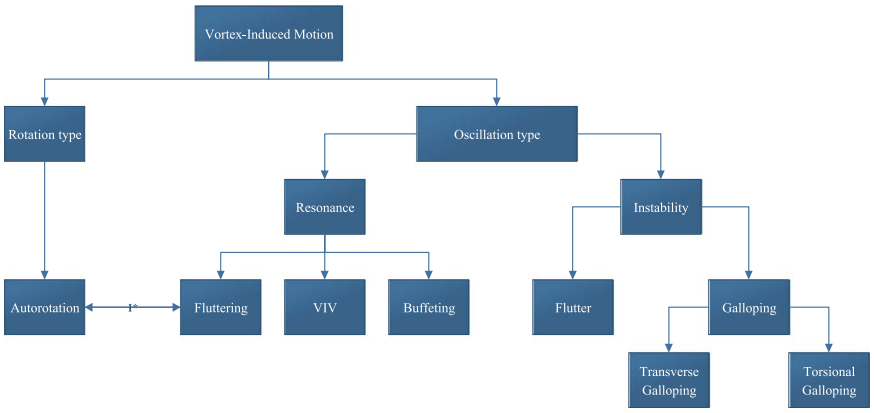

Fig. 1. Classification of vortex-induced motions.

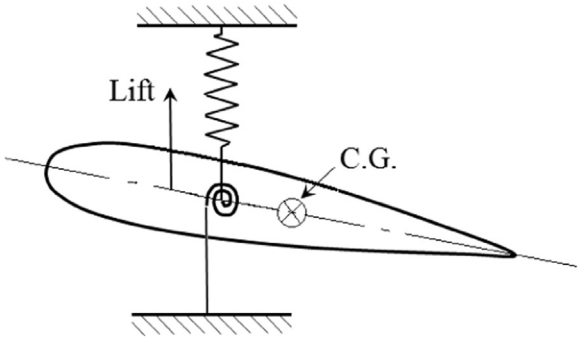

Fig. 2. Schematic of an airfoil in unstable condition.

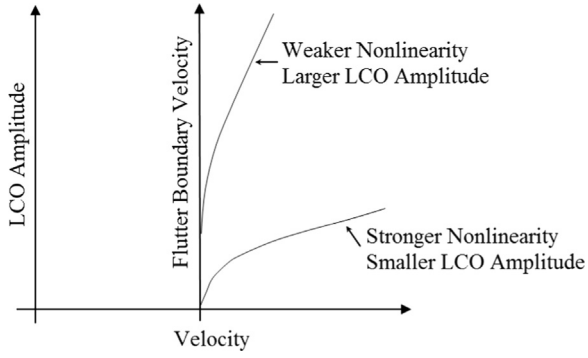

Fig. 3. Bifurcation plot of the amplitude-velocity of flutter phenomenon [11].

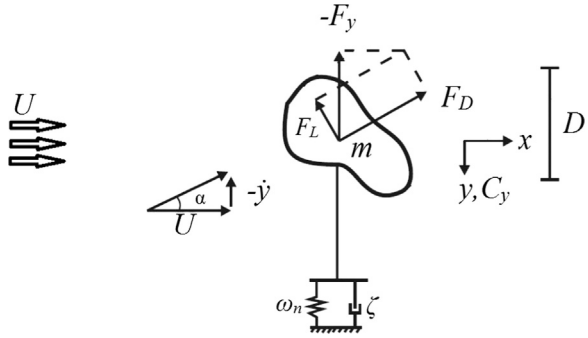

Fig. 4. Single DOF prismatic body connected to a linear spring, subjected to an incoming flow in the transverse direction.

transverse galloping. Taking the derivative of Eq. (3) in terms of α yields

$$\frac{dF_y}{d\alpha} = \left(F_L - \frac{dF_D}{d\alpha}\right)sin\alpha - \left(F_D + \frac{dF_L}{d\alpha}\right)cos\alpha \tag{4}$$

For $\dot{y} \gg 1$ and $\alpha \gg 1$, $sin\alpha \approx O(\epsilon)$, Therefore

$$\frac{dF_y}{d\alpha} \approx -\left(F_D + \frac{dF_L}{d\alpha}\right) \tag{5}$$

Thus, the criterion for galloping instability is

$$F_D + \frac{dF_L}{d\alpha} < 0 \tag{6}$$

Defining $F_L = \frac{1}{2}C_L\rho U^2 hl$ and $F_D = \frac{1}{2}C_D\rho U^2 hl$, and similarly for F_y, ρ being the fluid density, h a characteristic frontal dimension, and l the length of the prism perpendicular to the plane of the paper (the span), Eq. (6) may be rewritten in terms of the lift and drag force coefficients:

$$C_D + \frac{dC_L}{d\alpha} < 0 \tag{7}$$

This expression is known as Glauert-Den Hartog criterion for the onset of transverse galloping [15]. Furthermore, Van Oudheusden [16] has imposed essential condition as a negative fluid dynamic damping for happening of transverse galloping. Since the fluid force is considered as a contribution to the total damping of the system (fluid dynamic damping), negative lift coefficient derivative and negative fluid dynamic damping are equivalent [17]. To prove the similarity of these conditions, one may write the total damping coefficient as:

$$\zeta_T = \zeta + \frac{\rho U b}{4m\omega_n}\left(\frac{dC_L}{d\alpha} + C_D\right)\Big|_{\alpha=0} \tag{8}$$

Therefore, based on Van Oudheusden's condition, the oscillation will be stable if $\zeta_T > 0$ and unstable if $\zeta_T < 0$. As the mechanical damping ζ is generally positive, instability will only occur if $(\frac{dC_L}{d\alpha} + C_D) < 0$. From fluid mechanics, it's known that the drag coefficient of non-circular cross section in low angle of attack ($\alpha \ll 1$) is zero, thus the Glauert-Dog Hartog criterion is true if the lift coefficient derivative becomes negative. Generally, transverse galloping will happen if energy ratio becomes greater than 1.

As stated in former paragraph, the sufficient condition for transverse galloping is negative damping ($\zeta_T < 0$), and according to Eq. (8):

$$\left(\frac{dC_L}{d\alpha} + C_D\right)\Big|_{\alpha=0} < -\frac{4m\zeta\omega_n}{\rho U b} \tag{9}$$

The right hand side of Eq. (9) tends to zero when the velocity increases. In other words, the possibility of transverse galloping increases as velocity increases. Moreover, the discussed term tends to infinity when the velocity goes to zero. It states that transverse

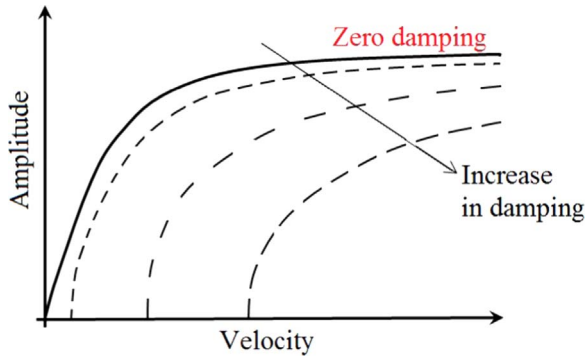

Fig. 5. Typical curve of the amplitude of transverse galloping with respect to velocity [16].

galloping will only be possible beyond a minimum threshold value of the incident fluid velocity [17]. This minimal value of U is known as the critical velocity for the onset of transverse galloping. Also, any increment in structural damping causes an increase in the critical velocity. In Fig. 5, the typical curve of amplitude-velocity of transverse galloping is shown. As demonstrated in this figure, transverse galloping is started in very low current velocity when structural damping is zero. Critical velocity corresponding to different structural damping clearly is shown in this figure.

In the transverse galloping phenomenon, the elastic body oscillates at much lower frequency than one of vortex shedding found in the Kármán vortex street [17]. Therefore, transverse galloping is not characterized as resonance type vibration. On the other side, due to oscillation of structure in low frequency, analysis of transverse galloping may adopt a quasi-steady approach. It means that at each instant the unsteady forces are taken equal to those occurring in an equivalent steady situation, with the same relative motion between structure and flow.

2.2.2. Torsional galloping

Torsional galloping is another typical instability, which induces torsional oscillation around a hinged axis of an elastic structure, due to aero/hydro dynamic loads into the cross flow. torsional galloping of elastic structures is of great importance in various engineering areas, mostly due to its destructive effects. For example, the Tacoma Narrows Bridge Collapse in 1940 was caused by torsional galloping, due to the negative damping in the torsional degree of freedom of the bridge deck [18]. However, torsional galloping can be driven into a controlled motion and be used to extract energy from the flow, becoming an alternative approach for wind and current power generation systems [19,20].

Torsional galloping is generally acknowledged to be significantly more difficult to analyze than transverse galloping. The aero/hydro dynamic forces for torsional galloping depend on both the angular displacement and the angular velocity, whereas for transverse galloping they depend only on the vertical velocity. In order to clarify more, consider a hinged rectangular plate undergoing torsional galloping as depicted in Fig. 6. The relative flow velocity along the chord length of the plate varies from point to point. This causes each point of the cross section to have a different translation vector, and hence a different local relative angle of attack. Another difficulty is that the phase difference between the fluid-dynamic forces acting on the section and motion of the section changes with flow velocity. No totally satisfactory solution has been found to these difficulties, and hence analytical models of torsional galloping involve approximations going considerably farther than the quasi-steady assumption.

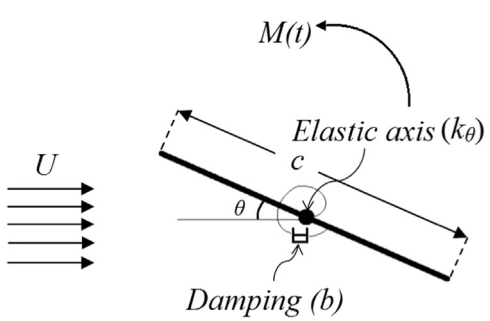

Fig. 6. Schematic view of the elastically supported rigid structure.

Several attempts have been made to model the rotation using linear quasi-steady approach [14], and nonlinear quasi-steady approach [4]. However, further statements showed that torsional galloping is an unsteady rather than quasi-steady phenomenon, due to what is called the fluid memory effect. The fluid memory effect is really a phase-lag effect which causes a part of the displacement-dependent force to be transformed into a velocity dependent one [13].

In order to clarify the unsteady theory, consider a one degree of freedom elastically supported rigid structure of length c, constrained to rotate into a cross-flow of speed U (see Fig. 6). The equation of motion of the structure is

$$I\ddot{\theta} + b\dot{\theta} + k_\theta\theta = M(t) \tag{10}$$

where I is mass moment of inertia, b is damping coefficient, k_θ is the torsional stiffness of the structure, $M(t)$ is the excitation moment, and dots mean derivative with respect to the time t. Given the fact that the hydro/aero dynamic forces on the structure will vary with the frequency of oscillation, the frequency-domain approach is widely used to model these forces and moments, by means of some frequency dependent coefficients known as flutter derivatives [21,22]. Hence the excitation moment can be written as

$$M(t) = \rho U^2 c^2 h\left(K\frac{c}{U}B_\theta\dot{\theta} + K^2 C_\theta\theta\right) \tag{11}$$

where B_θ and C_θ are the flutter derivatives, which are functions of frequency, $K=\omega c/2U$ is the reduced frequency, and ω is the is the response frequency of torsional galloping. Replacing $M(t)$ from Eq. (11), an K into Eq. (10) yields

$$\ddot{\theta} + \frac{1}{I}(b - 0.5\rho c^4 h\omega B_\theta)\dot{\theta} + \frac{1}{I}(k_\theta - 0.25\rho c^4 h\omega^2 C_\theta)\theta = 0 \tag{12}$$

This equation has two modes of instability. First one is the steady instability or divergence and occurs when the total stiffness term (coefficient of θ) falls to zero. To have divergence, it is necessary for C_θ to be positive. The second one is dynamic instability or torsional galloping and it occurs when the total damping (coefficient of$\dot{\theta}$) passes through zero. The necessary condition for torsional galloping to occur is that $B_\theta$must be positive.

It should be noted that, in order to obtain the required input data for this theory, i.e. the flutter derivatives, a major experimental effort is necessary. It should also be noted that the flutter derivatives contain all possible flow-induced excitations, including all vortex-shedding-related phenomena, and two degree-of-freedom Flutter.

2.3. Buffeting

Buffeting is a type of VIM caused by the unsteadiness of the incoming flow, which may be due to natural turbulence, or by the presence of the wake of upstream objects [23,24]. In order to illustrate better the mechanism of buffeting, consider a one-degree-of-freedom dynamic system undergoing some unsteady forces due to the fluid flow. The equation of motion for such a system can be written as

$$m\ddot{x} + C_{st}\dot{x} + kx = F_{MIM}(t) + F_{EIM}(t) \tag{13}$$

where m is the mass, C_{st} is the structural damping coefficient, k is the structural stiffness, and the dots are the derivatives with respect to time. The unsteady forces, generated by the fluid flow, have been

decomposed into two components, F_{MIM} and F_{EIM}. According to Naudascher and Rockwell's classification, F_{MIM} stands for the Movement-Induced Excitation. For flutter and galloping, F_{EIM}=0 [25]. Hence, these phenomena have been categorized as Movement-Induced Excitation problems because the force F_{MIM} on the right-hand side of Eq. (13) depends entirely on the structural response of the system and its time history [26]. On the other hand, for buffeting the response is driven by forces that are created by the oncoming vortices and are external with respect to the fluid-structure system, i.e. $F_{EIM} \neq 0$. Following Naudascher and Rockwell, this external system of forces (F_{EIM}) is denoted as an Extraneously-Induced Excitation (EIE) [25].

In general, the word buffeting is used to describe the response of the structure to an aero/hydro dynamic excitation which is created by a viscous phenomenon. This excitation, so called "buffet", is induced due to pressure fluctuation on the body surface and therefore can occur in any part alongside the body in the flow [27]. In order to induce buffet excitation into structures submerged in subsonic regime of the fluid flow, three main sources can be pointed out as:

1. Separation of the flow on the surface of the body.
2. Instability due to upstream obstacle such as vortex shedding from other bluff body.
3. Free stream turbulence due to meteorological phenomena

The first source of buffeting (buffeting due to flow separation) can be observed in aircrafts as dynamic response of wings to wide frequency band of excitation because of the flow separation on the wings due to flight in high angle of attack. About the second source, it is now established that there is a relationship of buffet to the classical flow field known as the Von Kármán vortex street that arises from wake oscillations behind a blunt body. This type of buffeting also is known as Wake buffeting. Wake buffeting is common in urban areas with many tall structures. The third source of pressure fluctuation of buffeting can produce significant vertical and torsional motions of a bridge even at low speeds. Therefore, it can be stated that buffeting may occur in wide range of flow speed. In other words, buffet has not critical onset velocity and also upper limited range. However in aeronautics, the onset of buffeting is crucial so far and researchers are trying to find a method to predict the onset of this phenomenon [27].

Buffeting is mostly dynamic in nature, because of which altering the stiffness or damping of the structure will not necessarily change the fatigue load [28]. Although the amplitude of oscillation due to buffeting is typically smaller than for VIV, the frequency range over which it can occur is greater, 0.1–60 Hz [13].

Rarely, buffeting was found to play a constructive role, for instance in biology. Recently, it has been found that a freshly killed fish is capable of moving upstream within the Kármán vortex street generated by a D-shape cylinder [29]. Furthermore, Beal et al. showed that live fish can swim upstream without any energy of their own; they extract the required energy from the oncoming large-scale vortices [30]. Their observation is also significant in the development of low-drag energy harvesting devices.

2.4. Vortex-Induced Vibration (VIV)

When an elastic bluff body encounters uniform fluid flow, for high enough Reynolds numbers (Re > 100), the flow separates from the body surface and generates an unsteady broad wake. This wake is recognized by two vortices in each side of the body which are shed into the current, periodically. This periodic vortex shedding generates asymmetric pressure distribution around the body that provides periodic forces which consequently lead to a limited amplitude vibration in the body. Koumoutsakos and Leonard [31] proposed the total force on a body (per unit length) in a viscous flow to be calculated as:

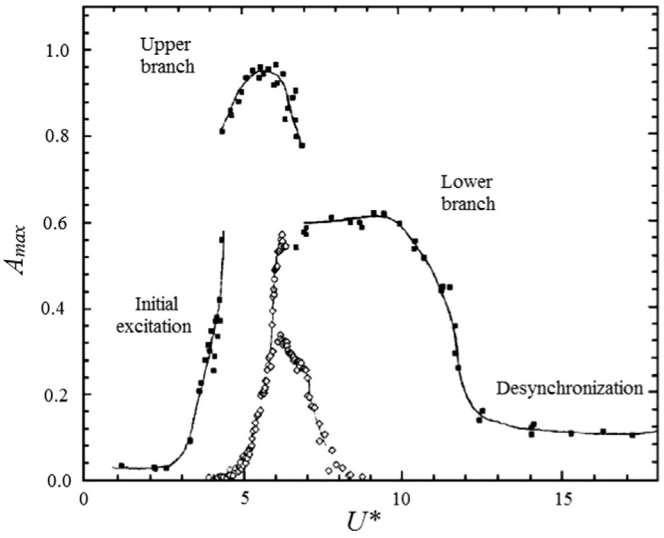

Fig. 7. Non-dimensional maximum amplitude of oscillation with respect to reduced velocity for VIV, filled squares are low mass ratio and damping and open squares are high mass ratio [32].

$$F_V = \rho \frac{d}{dt} \int (\omega_A \times x) dV + \frac{\rho \pi D^2}{4} \frac{dU}{dt} \tag{14}$$

where ω_A is the entire vorticity in the flow field minus "part of the distribution of vorticity attached to the boundary in the form of a vortex sheet [32]. Growth in vortex generation yields to increase ω_A which consequently enlarges total force according to Eq. (14). Hence, any increase in current velocity from zero causes an increase in the vortex shedding frequency. In a certain flow velocity, the frequency of vortex shedding is close enough to the natural frequency of the body in which the body oscillates in resonance regime [32]. This non-linear resonance phenomenon is known as Vortex-Induced Vibration (VIV).

The resonance in VIV is called lock-in, wherein significant oscillation is induced in the body if values of the mass and mechanical properties become sufficiently low [32]. Fig. 7 represents the reduced velocity ($U^* = U/Df_N$) vs. dimensionless amplitude (A^*=A/D) curve of VIV for low and high mass ratios.[2] As shown in this figure, free vibration of the body at low mass and damping is associated with the existence of an upper branch of high amplitude response, whereas this branch is not recognized in high mass ratio. The upper branch corresponds to Lock-in or synchronization in VIV.

VIV can be observed in many branches of engineering; in civil engineering, slender chimneys stacks, tall buildings, electric power lines or bridges, in offshore and ocean engineering, mooring lines of offshore structures, and under water pipe lines, and in mechanical engineering in the tubes of heat exchange devices can be given as examples.

2.5. Autorotation

Among all induced motions, one pair motion exists that varies from oscillatory rotation to continuous rotation if specific condition is provided. This pair motion is known as Fluttering-Autorotation motion. The phenomenon of Autorotation is defined as continuous rotation of a freely rotatable body in uniform flow without external sources [33] and [34] of supplied power, whereas the oscillatory rotation of this body is named Fluttering.

Vortex formation in suction side of the body's edge plays important role to produce enough exciting moment for inducing the rotation on the body. On the other hand, a body can exhibit proper autorotation

[2] The dimensionless number typifying the ratio of the mean density of the body to the density of the surrounding fluid.

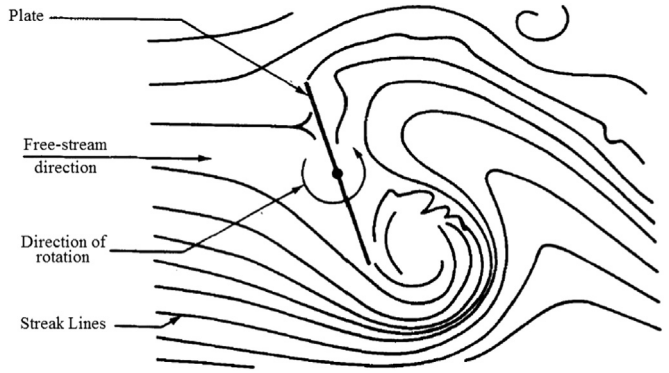

Fig. 8. Sketch from smoke-tunnel of an autorotating flat plate [35].

only if one or more stable positions exist at which the fluid flow exerts no torque on the resting body. These positions for flat plate are perpendicular and parallel to fluid flow. In these cases, a sufficiently strong impulse is required before the fluid flow can sustain a continuous spinning of the body. Such a strong impulse is provided by vortex shedding in perpendicular situation. For a flat plate rotating around an axis, a large vortex shed from the retreating face, while no similar vortex is visible from the advance face as shown in Fig. 8.

Autorotation occurrence in a body depends on its geometry. Lugt [36] has stipulated the different kinds of autorotation of various bodies. He stated that the flat plate and elliptic cylinder are not the only cylindrical bodies capable of autorotation. Riabouchinsky [37] reported the autorotation mode for the triple and cruciform plates by experiments. He found that the rate of rotation decreases with increasing the number of plates. In a more general work, Skew [38] has found that bodies with three sided cross section (triangles) autorotate faster than other cross sections. Although, spin of the flat plate and square cross section bodies is the same rate, but bodies with maximum seven sides (heptagons) show autorotation. In other words, octagonal cross sections and higher cannot reach to the state of autorotation.

Bifurcation from fluttering to autorotation occurs in specific amount of mass moment of inertia. The dimensionless moment of inertia (I^*) is defined as the ratio of mass moment of inertia of the system to its added moment of inertia. It formulates as $I^* = 32I_s/\pi\rho_w C^4 H$ where I_s, ρ_w, C and H are body geometrical moment of inertia, fluid density, chord and span lengths, respectively [3]. By enough large mass moment of inertia, fluttering motion (angular oscillation) is translated to autorotation (continuous rotation). However, a chaotic phenomenon may happen as a transition between the pure oscillation and the pure rotation. Bakhshandeh Rostami and

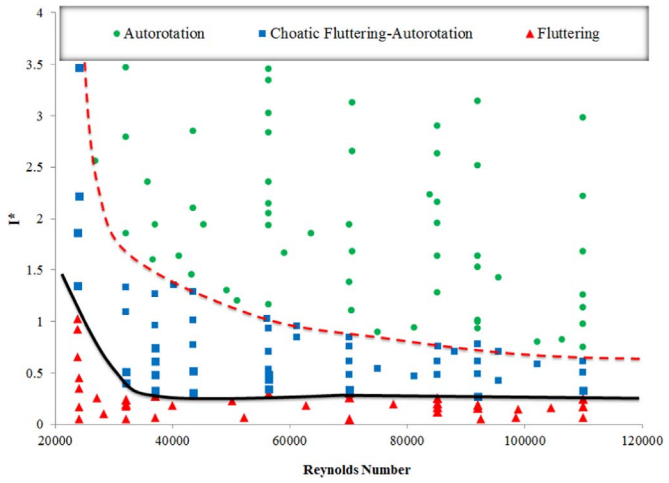

Fig. 9. Bifurcation diagram to classify different motions of flow induced rotation based on Reynolds number and dimensionless moment of inertia by experimental data [39].

Table 1
I* values corresponding to bifurcation of fluttering and autorotation obtained from experimental studies.

Investigator	Method (Physics)	Re (Medium)	Bifurcated I^*	Body cross section (AR)	Extra descriptions
Field et al. [41]	Falling (3 DOF)	20–30,000 (Water)	0.22	Circular disk (AR=1)	Different I* 0.04–2) has been revealed four regimes as steady, periodic, chaotic and tumbling for descending.
Belmonte et al. [42]	Falling (3 DOF)	3000–40,000 (water)	0.37	Thin flat strip (AR=∞)	Frictional effect was observed in their experiments.
Willmarth et al. [43]	Falling (3 DOF)	1– 19,000 (water)	0.17	Circular disk (AR=1)	Disks with different materials are descended freely into water and therefore, effect of friction was negligible. Autorotation will happen for Re > 2000.
Smith [44]	Hinged (1 DOF)	20,000–400,000 (Air)	0.19	Flat plate (AR=2–9)	For I* less than 0.1, the plate does not autorotate even in high Re. Friction vanished using air bearing.
Andersen et al. [45]	Falling (3 DOF)	1000 (Water)	Between 0.16 and 0.29	Flat plate (AR=∞)	They have pointed out only to I*=0.16 for fluttering and I*=0.29 for autorotation.
Mirzaeisefat and Fernandes [46]	Hinged (1 DOF)	3000–20,000 (Water)	0.28	Flat plate (AR=∞)	They have not reported the chaotic phenomenon.
Bakhshandeh Rostami [39]	Hinged (1 DOF)	2000–110,000 (Water)	0.22	Flat plate (AR=∞)	This I* has been reported in existence of bearing damping.

Fernandes [39] have obtained a bifurcation diagram for autorotation, chaotic and fluttering motions of a hinged flat plate by experimental data, as shown in Fig. 9. This diagram, which is presented based on I* against Reynolds number, shows that the bifurcation point from fluttering to autorotation is almost independent of Reynolds number, and it happens in I*=0.22, approximately. They have also reported the similar result [40] by numerical simulation. Their simulation shows also an independent manner of I* from current velocity and they have reported the bifurcation point in I*=0.162. Tables 1, 2 list the values of I* corresponding to bifurcation of fluttering and autorotation obtained by several experimental and numerical studies, respectively.

Table 2
I[a] values corresponding to bifurcation of fluttering and autorotation obtained from numerical studies.

Investigator	Equation (Physics)	Method of solution	Bifurcated I[a]	Body cross section (AR)	Simulated range of Re (and I[a])	Extra descriptions
Mittal et al. [47]	2D NS[a] (Falling)	Cartesian grid method	0.17	Rectangle - circular disk (AR[a]=∞ - 1)	50–600	
Andersen et al. [48]	2D NS (Falling)	vorticity–stream formulation	0.194	Ellipse (AR=∞)	400–600 (1.1–3)	They applied a body-fitted computational grid generated by a conformal mapping.
Andronov et al. [49]	2D NS (Hinged)	Meshless viscous vortex domain method	Between 0.1 and 0.2	Rectangular plate (AR=∞)	10–1000 (0–0.1–0.2)	This paper has generally considered the effect of I on autorotation characteristics.
Lugt [50]	2D NS (Hinged)	FD[a] scheme used to solve vorticity equation	0.152	ellipse (AR=∞)	Re < 400	In this work, angular velocity of body supposed to be constant.
Wu and Lin [51]	2D NS (Falling)	modified direct-forcing immersed-boundary	Between 0.12 and 0.35	ellipse (AR=∞)	10– 10,000 (0.08–0.6)	They classified five regimes as steady falling, transient steady to fluttering, fluttering, chaotic and tumbling.
Rostami and Fernandes [40]	ODE (Hinged)	Implicit time marching	0.162	Rectangular flat plate (AR=∞)	5000– 150,000 (0.01–0.4)	They have simulated by ORCAFLEX.

[a] NS: Navier Stokes, ODE: Ordinary Differential Equation, FD: Finite Difference, AR: Aspect Ratio.

3. Energy harvesting technologies based on VIM

As stated in the former section, the VIM phenomena occur due to the interactions between the elastic structure and the fluid forces. Due to these interactions, energy is transferred from the surrounding fluid to the structure. Such fluid-structure interactions might be destructive for cases like airplanes or bridges, but they provide an opportunity for innovative energy harvesting techniques via controling the VIM phenomena.

The energy harvesting efficiency (η) is defined by the ratio of the mean power attracted by the body from the flow (P_i) and the total power in the flow (P). Furthermore, form Betz-Lanchester theory, maximum attainable efficiency is 0.59 that is known as ideal efficiency for current turbine in unbounded condition (blockage effect tends to zero). Based on Betz-Lanchester, the maximum power extracted in a channel with the width W_{ch} and depth D_{ch} is defined as:

$$P_{max} \approx 0.59 \frac{\rho}{2} W_{ch} D_{ch} U^3 \tag{15}$$

In the following sub-sections, energy harvesting technologies using the VIM phenomena is reviewed.

3.1. Flutter

In a two degree of freedom wing undergoing flutter, or so called flutter wing, vortex shedding is synchronized with combinations of frequency of oscillation, heave amplitude and pitch angle. Because of low pressure core in the vortex; the process of vortex shedding creates higher pressure difference between both sides of the wing [52]. As a result, the flutter wing generates a high lift, which shows its great potential to harvest the energy.

The studies on flutter type energy converters can be classified into the following three categories with respect to the activating mechanism of the device [53]. First type is systems with forced pitching and heaving motions that, as shown in Fig. 10-a, is prescribed pitching motion θ(t) and heaving motion h(t). The second system is named semi-activated systems which is forced pitching motion to induce heave motion. These systems require controlling/actuating the pitching motion (see Fig. 10-b). Finally, third system which is shown in Fig. 10-c is known as self-sustained systems that the pitching and heaving motions are passive. In other words, these systems rely on flow-induced instabilities to generate oscillatory motions in the heaving and pitching directions [53].

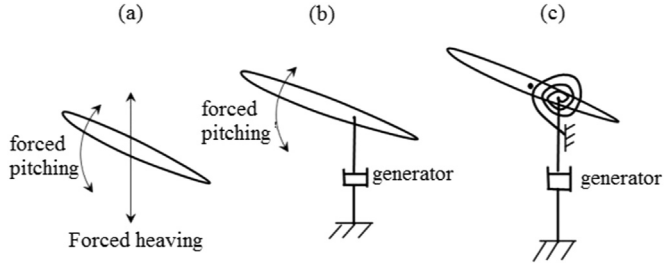

Fig. 10. Schematics of (a) a system with forced heaving and pitching motions, (b) a semi-activated system with forced pitching but induced heaving motions and (c) a self-sustained system with induced heaving and pitching motions, figure in courtesy of [53].

The performance or the efficiency of energy harvesting is defined as the portion of incoming flow kinematic energy flux extracted by the system. For flutter wing devices, the efficiency is formulated as:

$$\eta = \overline{P} / 0.5 U^3 Y_p S \tag{16}$$

where Yp is the difference between the highest and the lowest points reached by the foil, U is the speed of the incoming flow, ρ is the fluid density, s is the span length, and $\overline{P}$ isthe cycle-averaged power that demands special formulation for each type. For instance, the average of cyclic power for forced pitching and heaving motion system (Fig. 10-a) was formulated by Xiao and Zhu [53] as follow:

$$\overline{P} = \frac{1}{T} \int_t^{t+T} [Y(t)\dot{h}(t) + M(t)\dot{\theta}(t)] dt \quad Forced - oscillation \tag{17}$$

whereY(t)andM(t)are instantaneous lifting force and pitching moment, respectively and T is period of one cycle. As can be seen, in the first type, both motions of heave and pitch play positive roles in power generation. For semi-activated system, activation of pitch motion demands an input energy whereas the harvested energy is concluded by heaving motion. Thus, positive net energy extraction is possible when the energy extracted from the heaving motion is higher than the energy expenditure to activate the pitching motion [53]. Therefore, the averaged extracted power in one cycle by semi-activated system can be expressed by Eq. (18).

$$\overline{P} = \frac{1}{T} \int_t^{t+T} [C_0 \dot{h}^2(t) - M(t)\dot{\theta}(t)] dt \quad Semi - Activated \tag{18}$$

where C_0 is linear damping coefficient. By the same conclusion, Xiao and Zhu [53] have formulated the power extraction by self-sustained system as:

$$\overline{P} = \frac{1}{T} \int_t^{t+T} C_0 \dot{h}^2(t) dt \quad Self - Sustained \tag{19}$$

They only have supposed a positive role for heaving motion in power generation and ignored the effect of the pitch motion. Based on the discussion by Peng and Zhu [1], an ideal scenario is to insert the pitch motion in this formula as an energy harvester due to positive effect of torsional spring to produce oscillating moment. Thus, Eq. (19)

Table 3
Brief review of studies done on flutter foil.

Investigator	Method	Foil cross-section	AR	Re	reduced frequency f*	Heaving motion profile	η_{max} (%)
Ashraf et al. [55]	CFD	NACA 0014	∞ (2D)	20,000	0.8	Sinusoidal	34
Abiru and Yoshitake [56]	Exp.	NACA 0015	3	50,000	0.3	Induced	32–37
Huxham et al. [57]	Exp.	NACA 0012	3.4	45,000	0.025–0.2	Induced	23.8 at f*=0.1
Simpson et al. [58]	Exp.	NACA 0012	4.1, 5.9 and 7.9	13,800	0.2–0.6	Sinusoidal	43 at AR=7.9
Platzer et al. [59]	Exp. and CFD	NACA 0014	2.133	20,000	0.8	Sinusoidal	33
Usoh et al. [60]	CFD	NACA 0012 and plate	∞ (2D)	1100	0.6–1.2	Sinusoidal	P: 34.2 N: 32.5 at f*=0.80
Xiao et al. [61]	CFD	NACA 0012	∞ (2D)	10000	0.05–0.45	Sinusoidal and Non-sinusoidal	50
Hoke et al. [62]	CFD	NACA 0015	∞ (2D)	1100–20,000	0.14	Sinusoidal and Non-sinusoidal	37.3
Kinsey et al. [63]	Exp.	NACA 0015	7	500,000	0.12	sinusoidal	30

may be improved as:

$$\overline{P} = \frac{1}{T}\int_{t}^{t+T} [C_0\dot{h}^2(t) + k\theta(t)\dot{\theta}(t)]dtSelf - Sustained \quad (20)$$

where k is stiffness of torsional spring.

Young et al. [54], have reviewed the effect of different characteristics with the approach of fluid mechanics on the capability of energy generation by flutter phenomenon. Table 3 lists the studies which had result in energy extraction using flutter. The flutter airfoil systems are difficult to study experimentally, and therefore much work has been done to simulate the physics of flapping wing flight with Computational Fluid Dynamics (CFD). According to these studies which used symmetry foils, a foil with thick cross section can extract energy with higher efficiency. On the other hand, the highest efficiency by experiment was obtained in the highest aspect ratio. In other words, by increasing the span of oscillating foil, 3D effect decreases and as a result, the efficiency increases.

Growing importance of renewable energy caused to raise an interest in industries for developing prototypes of this novel concept in the past few years. As a result, some prototypes of energy harvesters have been developed based on the flutter phenomenon. The most famous prototype is the Stingray Tidal Stream Converter initially developed by the Engineering Business Ltd. (The Engineering Business Ltd. Technical Reports [64,65] and [66]) and further improved by Pulse Tidal Ltd. [67]. Stingray (see Fig. 11) uses a compensator arm for the power production from the sea flow. The efficiency of this model is 11% in the current speed of 2.5 m/s whereas the cut-in speed for this model is 1 m/s [66]. The base of this converter is anchored at the bottom of the sea to guarantee the stability. The compensator arm is fastened to a column on the base. By the undulation of the water, the fin of the compensator arm oscillates up and down. Thus, the pressure is generated inside a hydraulic cylinder which is used to power a generator. In the years 2002 and 2003 the equipment was tested with an installed rating of 150 kW as a pilot scheme [64,65]. In 2005, the enterprise Engineering Business Ltd had arrived at the conclusion that the equipment construction would possibly not be practicable in consideration of profitability and cannot continue to sustain this project and therefore have decided to put the Stingray project on hold [66].

Flapping wings, such as those used in nature by aquatic animals (such as Tuna, dolphin and shark) show great promise in novel flutter based energy extraction devices, due to their excellent hydrodynamic performance with high efficiency through the flapping motion of their caudal fins. bioSTREAM is the name of another flutter wing energy converter which has been inspired from Tuna and Shark tailfins and is being developed by Biopower systems (bps) Co. [68] for utility-scale power production from tidal currents. The currents on the ocean floor impose a force on the fin of the bioSTREAM device (see Fig. 12). The basic of bioSTREAM is semi-activated type of flutter wing energy conversion in which the pitching angle is forced. In other words, angle of attack of the fin is adjusted by an onboard computer perpetually to obtain maximum efficiency. The to-and-fro motion of the fin is directed into a specially designed gearbox that converts the oscillating motion into a rotational motion and drives a conventional dynamo. The minimum speed of current for operating of this design is 2.5 m/s [68]. The efficiency of this model has not been announced by BPS Co. but a 250 kW model is in development.

Tidal stream energy is not yet as developed as wind energy but has the advantage of being as predictable as the tides. Tidal energy devices do not have to be engineered to withstand storms and, as they are underwater, have minimal visual impact. Pulse Stream 100 [69] demonstrates an innovative shallow water tidal stream power generator which has been invented by BMT Renewables Ltd [70]. The Pulse Stream 100 (see Fig. 13) converter uses a pair of hydrofoils which oscillate across the tidal flow to enable the extraction of energy from shallow water of 10–30 m mean sea water level, an area not yet exploitable.

Another technology to use flutter for hydrokinetic energy extraction was introduced by the German company Aniprop (from a contraction of “Animal Propulsion”) [71,72]. They demonstrated an oscillating

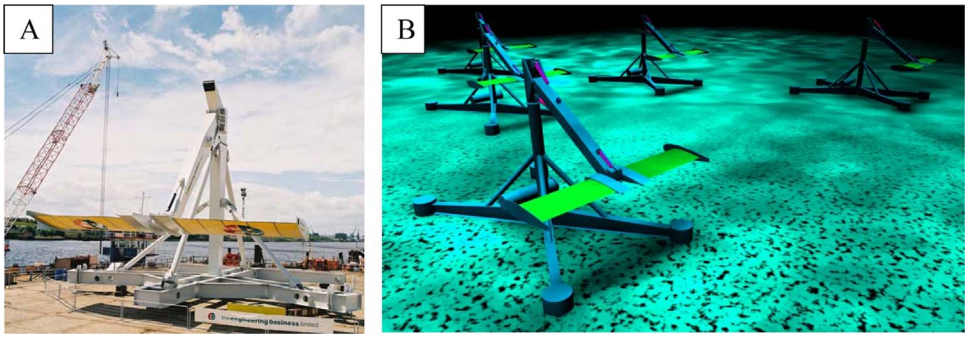

Fig. 11. (A) The Stingray before deployment for submerged testing (courtesy of Engineering Business), (B) Schematic of farm of Stingray project [67].

Fig. 12. bioSTREAM energy harvester [68].

hydrofoil power generator which extracted 1 kW from the river Lech in the city of Augsburg in 2004. In this turbine, the mechanism of the common sinusoidal pitch and plunge is substantially improved by introducing a "partially linear" motion. The device operated at f^*=0.11 and produced an approximate efficiency of η=8% [54].

Furthermore, Festo has developed a technology platform based on flutter which is called DualWingGenerator [73]. The system uses two pairs of opposing wings of NACA 0014 which are arranged on both side of the central column so that the pair of wings on one side forms a functional unit. When the fluid flows, the two slides move synchronously on the vertical guide in opposing directions: whilst the top two wings travel upwards, the bottom wings move downwards [see Fig. 14-left]. At the apex, a servomotor turns the wings and they automatically move back towards each other [see Fig. 14-right]. On the laboratory set-up, this system has achieved a remarkable efficiency of 45% in current velocity of 4 m/s. However, the efficiency decreases by increasing the current velocity and reaches to almost 30% in the velocity of 8 m/s. The power output of DualWingGenrator has been reported in the range of 40–100 W/m^2 for the velocity between 5 and 8 m/s [74].

3.2. Galloping

Some studies have proved the feasibility to extract useful energy from the surrounding flow, for the substantial galloping vibration. In this section, the studies about the energy extraction through galloping, both transverse and torsional, are reviewed.

3.2.1. Transverse galloping

Energy extraction via transverse galloping has been analytically and theoretically established through several studies. Barrero-Gil et al. reported an analytical study to prove the potential of transverse galloping in order to obtain energy [75]. Through their analysis, they described transverse galloping by a one-degree-of-freedom model considering the quasi-steady hypothesis. They investigated the influence of cross-section geometry and mechanical properties (synthesized in the product $m^*\xi$, the so-called mass-damping ratio) in the energy conversion factor of the model. However, specific methods on how to harvest this energy were not discussed in their work. Using the same physical principles, Sirohi and Mahadik proposed harvesting energy from transverse galloping of a prismatic structure that has an equilateral triangle section [76]. Their device consisted of surface-bonded piezoelectric sheets attached to two beams connected to the structure (see Fig. 15). They could generate more than 50 mW at a wind speed of 11.6 mph, using this device. Vicente-Ludlam et al. coupled the model presented at Barrero-Gil et al. [75] with a mathematical model of the electromagnetic generator [77]. They analytically calculated the dissipated current at a generic electrical load resistance, and by means of that they could estimate the capacity to produce electrical energy. However, they did not predict the output levels that can be harvested in their investigation.

Moreover, Vicente-Ludlam et al. [78] demonstrated theoretically that transverse galloping in a dual mass system will enhance the energy extraction efficiency. The dual-mass system promotes a broadening of the values of the incident flow velocities at which the efficiency is kept

Fig. 13. Designs and prototype of Pulse Stream 100 innovated by BMT Renewables Ltd [69].

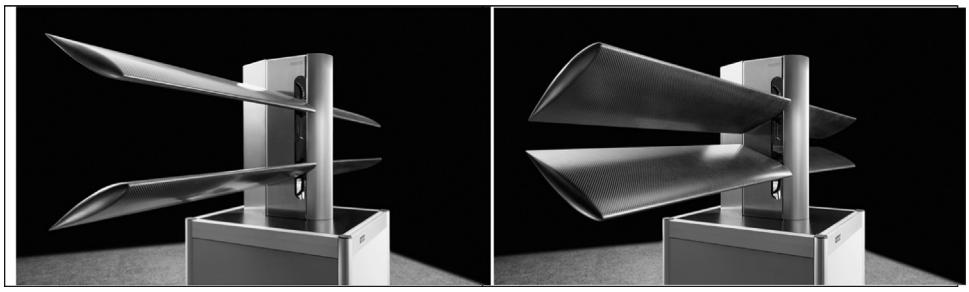

Fig. 14. Two modes of movements in DualWingGEnerator [73].

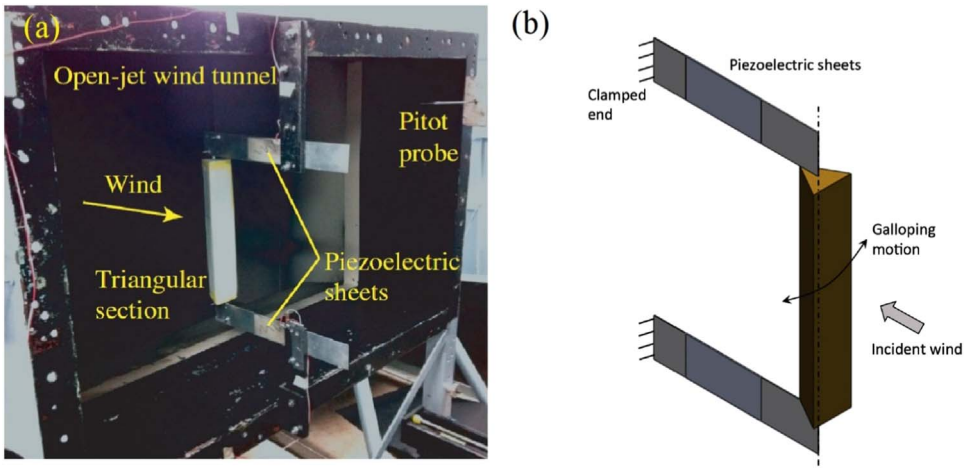

Fig. 15. Sirohi and Mahik transverse galloping based piezoelectric energy harvester device; (a) Prototype, (b) sketch [76].

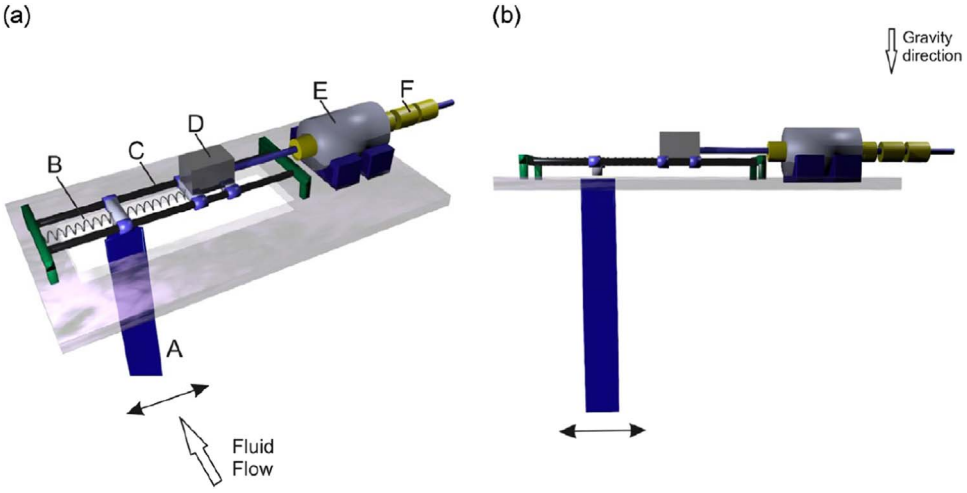

Fig. 16. Sketch of a potential practical realization of dual-mass system transverse galloping energy harvester presented by Vicente-Ludlam et al, including a galloping prism (A), springs (B), a linear guide (C), transverse the flow direction, the secondary mass(D), the stator (coil) part the electromagnetic generator (E) , and a permanent magnet array (F). A 3D view is shown in (a) whereas a front view is shown in (b) [78].

Table 4
Brief review of studies on regarding energy extraction through transverse galloping.

Investigator	Method (Fluid)	Re (Re=UD/v)	Aspect ratio	Mass-damping ratio (m*ξ)	Reduced velocity	η_{max} (%) (description)
D. Vicente-Ludlam[77]	Analytical (Air)	68,000	5	3.36	34	51
D. Vicente-Ludlam et al. [78]	Analytical (Water)	5032 (Dual mass) 2516 (Single mass)	20	1.25	12.66 (Dual mass) 6.33 (Single mass)	49 (Dual mass) 43.8 (Single mass)
Sirohi and Mahadik [76]	Experimental (Air)	13,210	6.275	m* not given (ξ=0.015)	4.6155	6
Dai et al. [81]	Analytical (Air)	76,400	2D (D=0.03 m)	m* not given (ξ=0. 0013)	4.42	1.56
Ewere et al. [82]	Experimental (Air)	9550	2	0.32	–	1.8

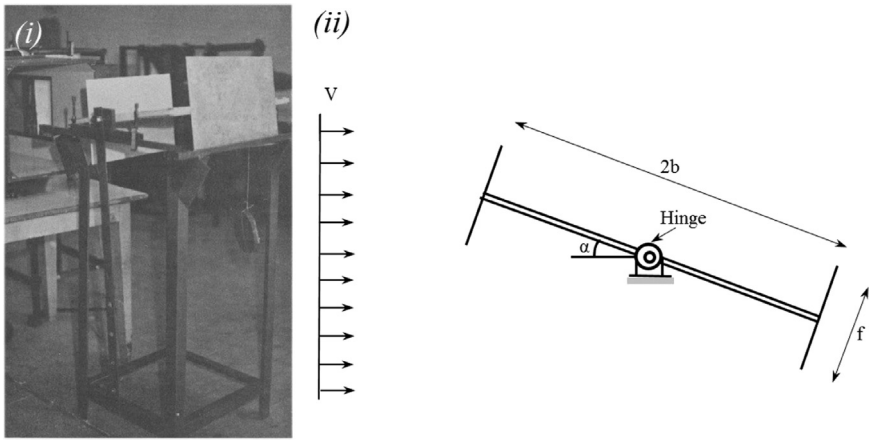

Fig. 17. Ahmadi's model for wind energy extraction via torsional galloping; (i) Picture, (ii) Sketch. [20].

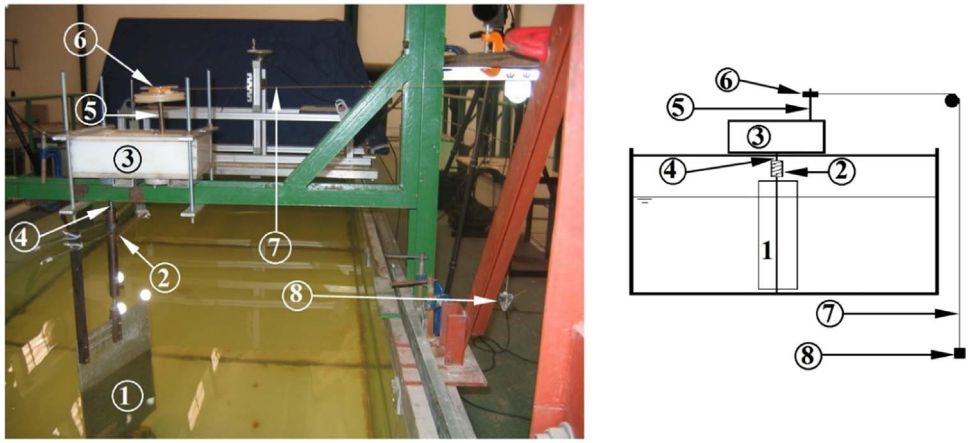

Fig. 18. Test set-up for hydrokinetic energy extraction through torsional galloping; (Left) A photograph of the water current energy extraction set-up in LOC, (Right) Schematics front view; The tags: (1) The flat plate, (2) The torsion springs, (3) The transmission system, (4) The input shaft, (5) The output shaft, (6) The sheave, (7) The string, (8) The weight [21].

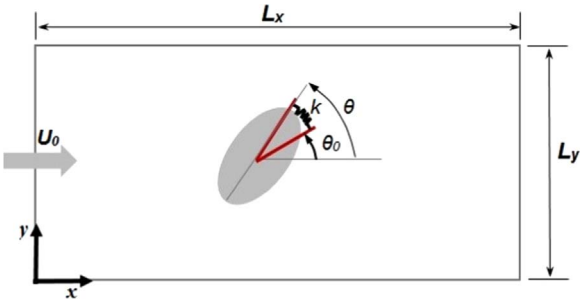

Fig. 19. Schematic of setup. Uniform flow with velocity U_0 is applied at the inlet ($x = 0$). At a given instant in time, the major axis of the ellipse is oriented at an angle θ w.r.t. the x direction, and $\theta_0$is the equilibrium angle of the torsional spring. Torque acting on cylinder due to the spring is$-k(\theta - \theta_0)$. Convective boundary condition is applied in other three directions [83].

high. For illustration purposes and gain better physical insight, they presented a potential practical implementation of dual-mass system in their article (see Fig. 16). They explained their system in operation as follows: under the action of the fluid flow, the galloping body oscillates perpendicular to the direction of the flow and drives the secondary mass (or dual mass). This secondary mass then drives the permanent magnet of a linear electromagnetic generator. A dual-mass system can be implemented in the built transverse galloping energy harvester with small changes. The changes include only the introduction of a secondary mass and reorganizing the elements that had already been installed in the original single mass system. Then, it is possible to improve the maximum efficiency that can be harvested as well as to broaden the range of reduced velocities where such efficiency is kept high.

The influence of the bluff body cross section geometry on the

Table 5
Brief review of studies on regarding energy extraction through torsional galloping.

Investigator	Method (Fluid)	Re (Uc/ν; c is chord length)	Aspect ratio (chord to span)	Axis position (from the L.E.)	Reduced velocity ($U_r = \frac{U}{\omega_n C}$)	η_{max} (%) (description)
Ahmadi[20]	Experimental (Air) Theoretical (Air)	4×10^5	0.39	0.5	4.06	1.1 1.38
Fernandes and Armandei[21]	Experimental (Water)	10^5	0.44	0.5	3.3	1.8
Armandei and Fernandes[84]	Experimental (Water)	1.25×10^5	0.5	0.75	2.5	3.5
Bhattacharya and Sorathiya Shahajhan[83]	Numerical (Air)	200 100	2D	0.5	–	1.7 0.8

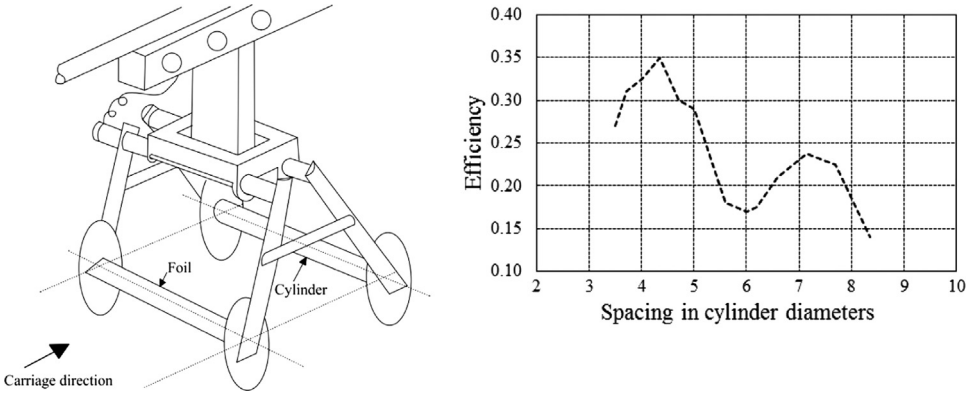

Fig. 20. Left: Experimental set up, Right: Apparent foil efficiency as function of spacing between cylinder and foil. A/d =0.833 and θ=45° [85].

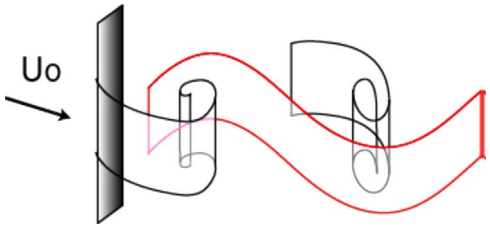

Fig. 21. Energy Harvesting Eel; Schematics [87].

performance of the transverse galloping energy harvesters should be taken into account, due to the fluid-structure interaction that leads to higher limit cycle oscillation amplitude. Ewere and Wang developed a coupled aero-electro-mechanical model to analyze a galloping piezoelectric energy harvester; with tip bluff bodies either rectangular or square section [79]. In another study, Zhao et al. experimentally investigated the effects of different tip bluff body sections on a transverse galloping piezoelectric energy harvesters, in which the square section, 3/2 and 2/3 rectangle sections, and equilateral triangle section are assumed [80]. In both studies, the square section outperformed the other sections in terms of harvested power. The square section bluff body shows a hysteresis in its limit cycle oscillation response, which is due to the unique feature of its vertical aerodynamic force.

The dynamical and the structural analyses of the transverse galloping were assessed through some studies, as they are related to the energy extraction performance. Dai et al. presented a nonlinear model to determine the effects of the load resistance and the wind speed on the transverse displacement amplitude, and power extracted by electromagnetic induction [81]. Furthermore, Ewere et al. suggested to use impact bump stop to improve the performance of the transverse galloping energy harvester by reducing the amplitude of the limit cycle while maintaining comparable harvested power [82].

A brief review of studies regarding energy extraction via transverse galloping is listed in Table 4. Except the analytical study conducted by Vicente-Ludlam et al. [78], wherein the transverse galloping energy

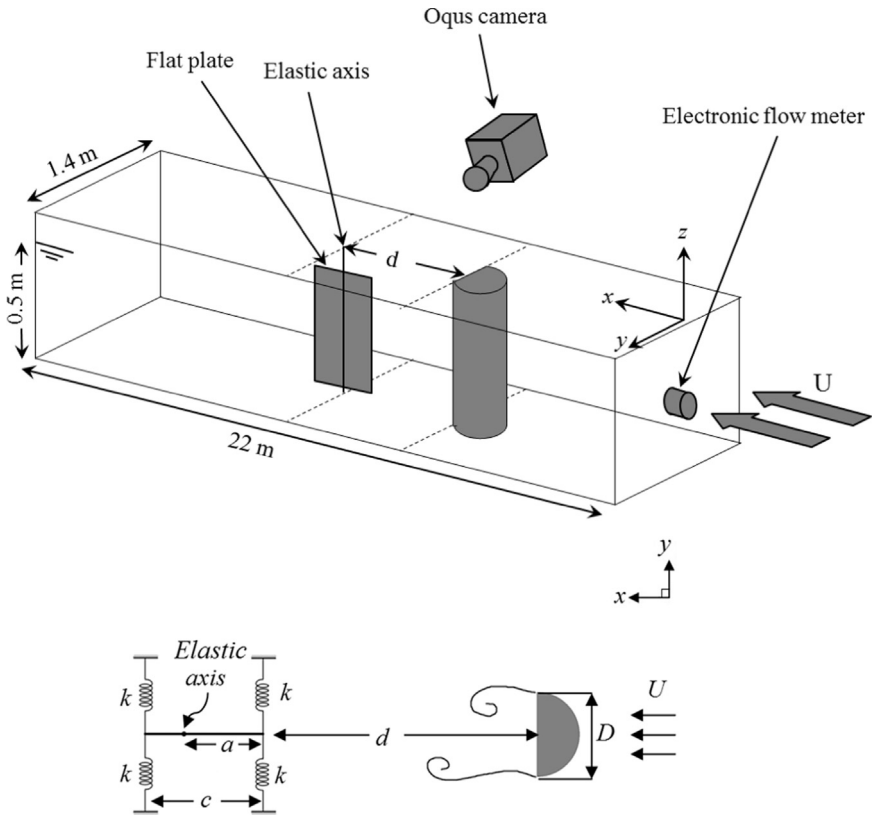

Fig. 22. Buffeting unit turbine for water current energy extraction; (a) Current flume layout with the arrangement of the instruments, and (b) Schematic top view [23].

Table 6
Brief review of studies on regarding energy extraction through buffeting.

Investigator	Method (Fluid)	Re	St (Definition)	Buffeting energy usage	$\eta_{max}(\%)$
Gopalkrishnan et al. [85]	Experiment (Water)	0.2×10^5	0.2 ($\frac{fd}{U}$)	Thrust production	35
Beal et al. [30]	Experiment (Water)	0.6×10^5	0.04 ($\frac{2H\omega}{2\pi U}$)	Thrust production	–
Taylor et al. [89]	Experiment (Water)	0.4×10^5	0.16 ($\frac{fD}{U_{inf}}$)	Power generation	37
Shen and Zhu[90]	Numerical (Air)	10^5	0.004 ($\frac{f_nD}{U}$)	Power generation	42.3
Armandei and Fernandes[23]	Experiment (Water)	0.75×10^5	0.4 ($\frac{fc}{U}$)	Power generation	60

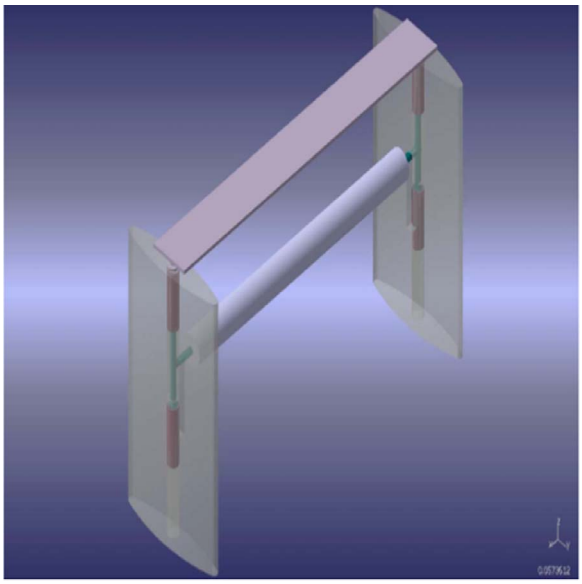

Fig. 23. VIVACE (Vortex Induced Vibration Aquatic Clean Energy) [92].

harvester is immersed in water, in all of the studies the fluid is air. Depending on the fluid, the applied Reynolds number's value is variable; low Reynolds numbers are applied for analytic researches when the fluid is water, intermediate Reynolds numbers are applied for the experimental researches in air, and high Reynolds numbers are applied for analytic researches when the fluid is air. Low aspect ratios are applied in air in comparison with water. The obtained maximum efficiencies by experiments are smaller than those obtained analytically. Furthermore, the maximum obtained efficiency depends on applied damping ratio.

3.2.2. Torsional galloping

Unlike transverse galloping, a few studies exist to report the results of the attempts to extract energy via torsional galloping. First attempt

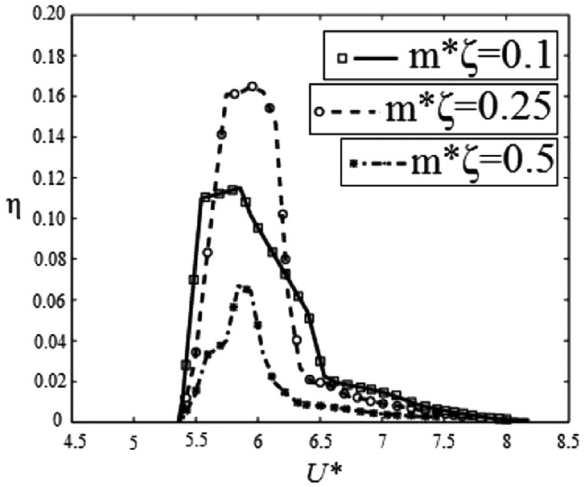

Fig. 25. Dependency of energy efficiency to mass-damping parameter [94].

was made by Ahmadi [20] who introduced the principle of aeroelastic wind energy conversion and described a model working based on torsional galloping. He constructed a small model of an aeroelastic wind energy converter and tested in a wind tunnel. The cross-section of the model resembles an H-section bridge deck (see Fig. 17). Thereafter, Fernandes and Armandei [21] conducted studies to investigate the capability of hydrokinetic energy extraction using torsional galloping by their invented device. Fig. 18 shows a photograph and a front view schematic of the hydropower extraction test set-up. Also, Bhattacharya and Sorathiya Shahajhan [83] performed a numerical study on the power extraction from torsional galloping of an elliptical cylinder. Their set up, an elliptical prism attached to a torsional spring, is schematically depicted in Fig. 19. Using the Lattice-Boltzmann method to simulate the fluid flow and fluid–structure interaction, they measured the potential for power-extraction from this set up, for different damping coefficients, solid-to-fluid density ratios and Reynolds numbers.

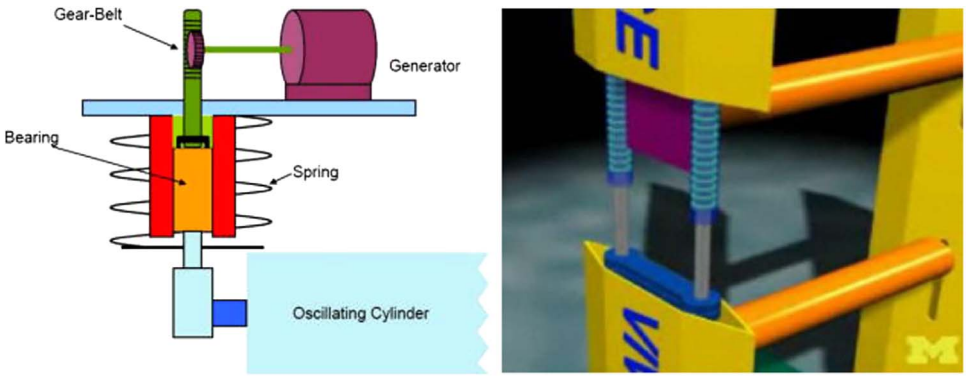

Fig. 24. Mechanical configuration for converting the oscillation to electricity in VIVACE [93].

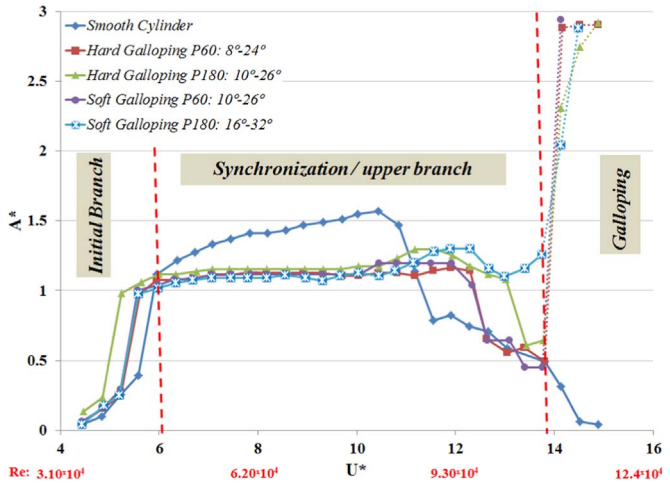

Fig. 26. Normalized amplitude with respect to normalized velocity of circular cylinder with and without PTC (different regime of oscillation has been indicated at m*=1.725 and $m^*\zeta$=0.0273) [96].

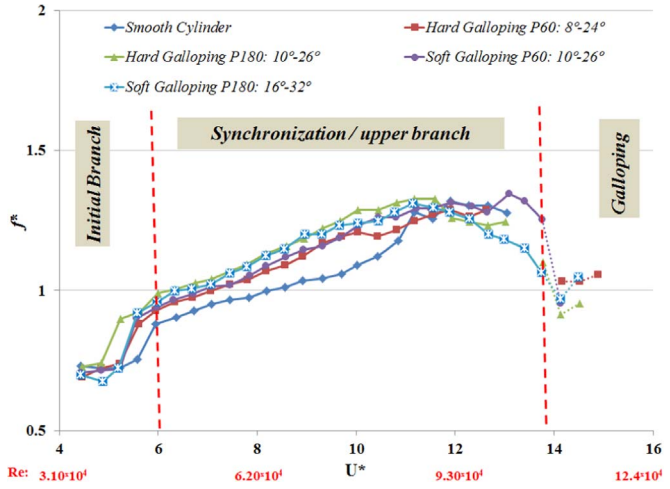

Fig. 27. Normalized frequency with respect to normalized velocity of circular cylinder with and without PTC at m*=1.725 and $m^*\zeta$=0.0273 [96].

In the studies of Ahmadi [20] and Fernandes and Armandei [21], the mathematical formulation presented to predict the power coefficient of the torsional galloping energy converter device relies upon the linear oscillation (Eq. (12)), whereas Bhattacharya and Sorathiya Shahajhan [83] consider the quasi-steady torque due to the fluid flow, as the Reynolds number is small. Furthermore, the physical work required to measure the energy extraction capability in Ahmadi [20] and Fernandes and Armandei [21] studies was chosen to be lifting weights up to a prescribed height, whereas for Bhattacharya and Sorathiya Shahajhan [83] it is measured by measuring the net dissipation rate in an externally attached angular damper.

One of the observations through the work of Ahmadi [20] was that the efficiency decreases with an increase in wind velocity. This was observed through the work of Fernandes and Armandei [21] as decrement of efficiency by increasing reduced velocity ($U_{r_n}=U/f_n c$). On the contrary, the trends from the simulation and analysis of Bhattacharya and Sorathiya Shahajhan [83] indicate that the efficiency of energy output should be higher at larger Re. It should be noted that their study only is conducted in low Re, i.e. laminar flow.

The investigations regarding energy extraction through torsional galloping are listed briefly in Table 5. It can be seen that the maximum efficiency obtained from torsional galloping based energy extraction reported to be very small, in turbulent flow [20,21]. Armandei and Fernandes [84] reported an almost 100% improvement in the performance of their torsional galloping based hydrokinetic turbine by optimizing the elastic axis position. Ahmadi [20] had a discussion on the effect of flange size on the performance from which he concluded that the 0.15 m is the optimal flange size. Bhattacharya and Sorathiya Shahajhan [83] demonstrated the efficiency variation with some parameters such as density ratios, ellipse aspect ratios, and lock-in of the fluid and solid oscillations.

3.3. Buffeting

As it was mentioned in section 2.3, energy extraction through buffeting can be significant in the development of low-drag energy extraction devices. The energy extracted via these devices can be used mechanically, say for thrust production, or electrically, say to harvest power from their surroundings.

3.3.1. Thrust production

The buffeting thrust generation mechanisms are generally based on the interaction between oncoming vortices from the upstream and the structure's oscillation. Gopalkrishnan et al. [85] investigated the vorticity control of an oscillating foil in order to improve its propulsive performance. According to the terminology defined here, their work can be categorized as buffeting. Their study relied on directly controlling the coherent vortices present in high Reynolds number flows. They placed a pitching and heaving foil in the wake of an oscillating D-section cylinder, and far enough to avoid the interference with the vortex shedding process (see Fig. 20-Left). They demonstrated that the peaks in the thrust generation efficiency, and hence energy extraction by the foil from the cylinder eddies, are associated with the destructive interaction, (see Fig. 19-Right). Destructive interaction is the formation of a street of vortices with circulation decreased through merging of cylinder vortices with vortices of the opposite sign shed by the foil [85].

While in earlier experiments the foil was actively oscillated behind the cylinder and the effect of energy extraction was documented in terms of an increase in its propulsive efficiency, Beal et al. [30] showed conclusively that a streamlined body passively oscillating within a vertical wake can extract sufficient energy from the turbulent eddies to

Table 7
Brief review on energy harvesting by VIV.

Investigator	Method (Fluid)	Re	Cross section	Optimum m*ζ	A^*_{max} (at Re)	f^*_{max} (at Re)	η_{max} (%) (at Re)
Ding et al. [98]	2D CFD (Water)	10,000–130,000	Q-trapazoid	0.076	3.5 (120,000)	1.1 (70,000)	45.7 (60,000)
Ding et al. [98]	2D CFD (Water)	10,000–130,000	Triangle	0.076	3.5 (130,000)	0.85 (80,000)	20 (50,000)
Ding et al. [98]	2D CFD (Water)	10,000–130,000	PTC- circular	0.076	3.5 (110,000)	1.2 (80,000)	37.9 (60,000)
Chang et al.[97]	Exp. (Water)	30,000–120,000	PTC circular	0.0212	3 (100,000)	1.3 (70,000)	≈ 43[a] (100,000)
Lee and Bernitsas[95]	Exp. (Water)	40,000–120,000	Circular	0.07	1.8 (118,000)	1.2 (100,000)	33.23 (80,000)
Barrero-Gil et al.[94]	Analyt.	1000	Circular	0.25	0.55	–	18
Bernitsas et al.[93]	Exp. (Water)	44,000–134,000	Circular	(m*=1.45)	1.4 (92,000)	–	22 (92,000)
Park et al.[96]	Exp. (Water)	30,000–12,0000	PTC circular	0.0277	2.9 (110,000)	1.3 (93,000)	≈ 35[a] (110,000)

[a] The efficiency has been calculated by Eq. (15) with φ=30°.

Fig. 28. Closed up view of VAACT- Left: flat plate shape type, Right: Flapped plate type (S shape type) [34].

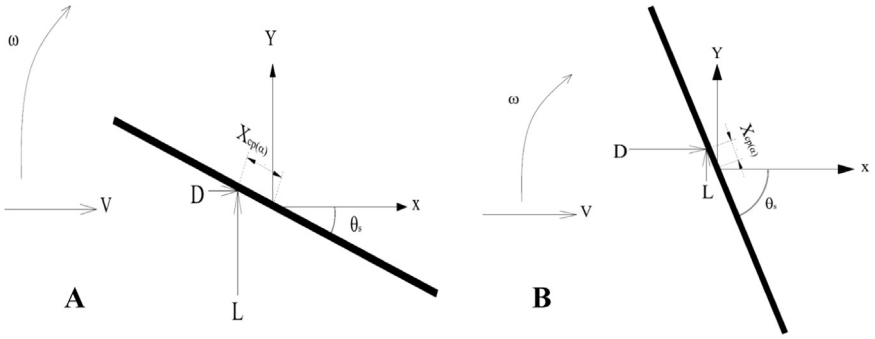

Fig. 29. Diagram of the hydrodynamic forces on the VAACT in low (A) and high (B) angle of attacks (L: Lift Coefficient, D: Drag Coefficient, Xcp: Center of pressure).

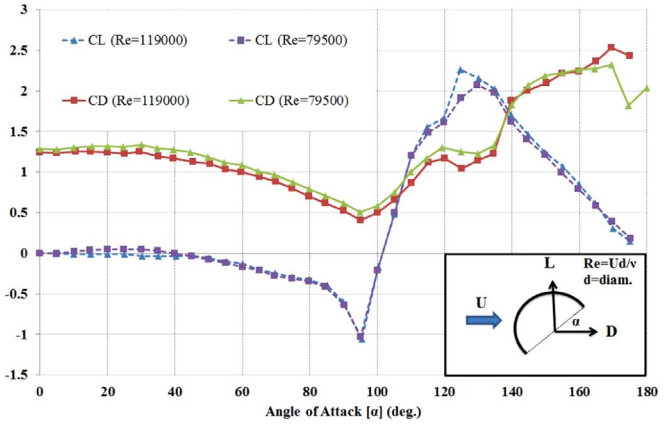

Fig. 30. Hydrodynamic coefficients of a semi-circular section [102].

propel itself upstream. Through their experiments, using the same apparatus as Gopalkrishnan et al. [85], they showed that a passively high aspect ratio foil can propel itself upstream when it is in resonance with oncoming vortices formed in the wake of a bluff cylinder. The positive axial force generated at negative power demonstrated that the foil extracts energy and simultaneously generates sufficient thrust to overcome its drag.

3.3.2. Power harvesting

Some studies use the piezoelectric materials as the technique to harvest energy from buffeting. Energy Harvesting Eel is a famous device to extract energy from buffeting using the piezoelectric technique (see Fig. 21). It consists of a piezoelectric membrane or "eel" placed in the wake of a bluff body, and the oscillation is induced from the von Kármán vortex street forming behind the bluff body in the membrane. Allan and Smith [86] studied the feasibility of extracting energy from Energy Harvesting Eel. Their data showed that the membranes are able to exhibit lock-in behavior to the bluff body shedding. In this case, lock-in or resonance is defined to occur when the membranes oscillate at the same frequency as the undisturbed wake behind the bluff body. The resonance was recognized as the ideal coupling or, wherein the membrane has a negligible damping effect on the von Kármán vortex street, and its amplitude will remain constant. It was anticipated that 1 m^2 of membrane should be capable of producing 1 watt of power [88].

Other aspect of Energy Harvesting Eel such as the interactions between the hydrodynamics of the water flow and structural elements of the Eel, through the mechanical energy input to the piezoelectric material, and finally the electric power output delivered through an optimized resonant circuit were modeled and tested by Taylor et al. [89]. They demonstrated the complete Eel system, with a generation and storage system, in a flow-tank testing, and obtained 37% of maximum efficiency.

Another technique that has been reported in order to harvest energy from buffeting relies upon electromagnetic damper cum. Shen and Zhu [90] demonstrated the effectiveness of the dual-function electromagnetic damper cum energy harvester through a numerical case study of bridge stay cables under buffeting vibration. They demonstrated that the overall energy harvesting efficiency for the wind speed ranges from 5 to 25 m/s, averages 42.3% at the optimal wind speed range (9–15 m/s).

Some studies on the feasibility for water current energy extraction via buffeting are also reported. Armandei and Fernandes [23] designed a preliminary unit turbine model, which works based on the buffeting phenomenon. The unit turbine model consisted of a rectangular flat plate hinged to an elastic axis along its chord and located in the wake of a D-section cylinder. They conducted several tests on this set-up in the current flume. The current flume layout with the arrangement of the instruments and the schematic top view of the set-up are shown through Fig. 22. Through the experiments, they observed that the position of the elastic axis, the distance d, and the elasticity k (see Fig. 22), play an effective role on the efficiency of the buffeting unit turbine. Nevertheless, their main observation was that oscillations close to the resonance improve the efficiency significantly, such that in one case they obtained 60% efficiency. Also, they estimate that a farm of 100 unit buffeting hydrokinetic turbines that work in their optimized situation can have a remarkable performance.

Table 8
Literatures review on the Autorotation based turbines.

Fernandes and Rostami[111]	Rostami and Fernandes[110]	Golecha et al. [109]	Golecha et al. [108]	Dobrev and Massouh[107]	Saha and Rajkumar[106]	Kamoji et al. [105]	Damak et al. [104]	Sarma et al. [103]	**Investigator**
Exp. (2D)	Exp. (2D)	Exp. (2D by using end plate)	Exp. (2D by using end plate)	CFD (2D) Exp. (3D)	Exp (2D)	Exp. (2D by using end plate)	Exp. (2D)	CFD Exp.	**Method**
Flat Plate (1, Rectamgle)	Flat Plate with two end flaps (1, Flat S)	Straight Savonious with deflector (2, semi-circle)	Straight Savonious in tandem configuration (2, semi-circle)	Straight Savonious, (2, semi-elliptic)	Helical Savonious with twisted angle of 0–25 degrees (2, semi-circle)	Helical Savonious with twisted angle of 90 degrees (2, semi-circle)	Helical Savonious with twisted angle of 180 degrees (2, semi-circle)	Straight Savonious, (3, semi-elliptic)	**Turbine type (Blade Number , Blade Cross section)**
0.5×0.3×0.005 (AR=1.66)	0.5×0.3×0.005 (AR=1.66)	0.17×0.245×0.002 (AR=0.7)	0.17×0.245×0.002 (AR=0.7)	0.2×0.2195×0.001 (AR=0.91)	0.22×0.24×? (0.916)	(0.211–0.224)× (0.202–0.253)× 0.003 (AR=0.88–1.2)	0.2×0.314×? (AR=1.57)	0.17×0.26 ×0.015 (AR= 0.65)	**Dimension {h×D×t} (m) (Aspect Ratio)**
0.21	0.21	0.15	0.15	0.133	0.64	0.39	0.50	0.21	**Blockage Ratio**
24500– 100,000 (Water)	20,000– 82,000 (Water)	20,000 (Water)	1,200,000 (Water)	40,000– 170,000 (Air)	103,000– 159,000 (Air)	57,700– 202,000 (Air)	80,000– 147,000 (Air)	79,000– 238,000 (Water)	**Re (medium)**
0.512	0.862	Single :0.7 Defl.: 0.82	Single: 0.7 Tandem: 0.8	0.8	0.65	0.17	0.4–0.45	0.77 (CFD and Exp)	**λ at η_{max}**
0.21 (Re= 60,000)	0.075 (Re= 21,000)	Re= 132,000	Re= 20,000	7.2	8.23	14	11.1	0.65 (Re= 172,000)	**U at η_{max}**
7	33.2	Single: 14 Defl..: 21	Single: 14 Tand.: 14 (gap=8)	Exp: 18 CFD: 20.8	14	20	25	40 (CFD) 39 (Exp)	**η_{max}**
1: appropriate range of Reynolds number is 40000– 70000. 2: the optimum value of I* is in the range of 0.5–0.6.	1: Extra moment of inertia on the turbine causes to improve the operation for harnessing energy. 2: Optimum range of moment of inertia is 0.6–0.7.	Maximum coefficient of power improves by 42%, 31% and 17% with deflector plate for two stage 0º phase shift,90ºphase shift and three stage modified Savonius rotor respectively.	1: Different tandem gap ratio of 3–8 has been investigated. 2: Performance of downstream turbine is comparable with upstream turbine if gap ratio is greater than 8.	1: All the computations are performed using the Navier-Stokes solver ANSYS Fluent 12.1. The model of turbulence is k-ω□SST.	1: From the performance viewpoint, twist angle of 15 is superior at lower wind velocities, whereas the twist angle of 12.5 is suitable at higher velocities.	1: They have investigated the effect of overlap ratio and aspect ratio on the performance of the turbine. 2: The helical angle is 90 degrees.	1: Helical degree was changed 0 in based to 180 at top of blade. 2: Maximum power coefficient of helical savonious turbine is higher than conventional one.	1: Power extracted by water is 62% higher than air in the same current speed. 2: CFD has been done by Fluent with approximately 196,000 meshes.	**Explanation**

Table 9
Selected turbines for different phenomena.

Case No.	Phenomenon Type	Turbine Name	Chord [m]	Span [m]	Swept Area [m^2]	Swept Volume [m^3]	Operational Re (U [m/s])	Efficiency η	Rated power [MW/y]
1	Autorotation	VAACT	0.3	0.5	0.15	0.143	74,700 (0.259)	15	6.16
2	Autorotation	Savonious (3 Elliptic Blades)	0.26	0.17	0.044	0.036	172,000 (0.655)	39	76.01
3	Autorotation	Savonious (Tandem)	0.245	0.17	0.041	0.032	20,000 (0.485)	14	10.32
4	VIV	VIVACE	0.125	0.914	0.342	0.042	92,000 (0.729)	22	177.4
5	Flutter	Flutter (Dual Foil)	0.24	1.68	1.03	1.33	500,000 (2.0)	30	3890.1
6	Flutter	Flutter (Single Foil)	0.24	1.68	1.03	0.247	500,000 (2.0)	20	2593.9
7	Torsional galloping	Torsional galloping	0.25	0.5	0.1963	0.041	125,000 (0.495)	3.5	0.84
8	Transverse galloping	Transverse galloping	0.04	0.251	0.0151	0.0007	13,210 (0.327)	6	1.67
9	Buffeting	Buffeting	0.3	0.5	0.0822	0.053	75,000 (0.248)	60	88.69

The investigations regarding energy extraction through buffeting are briefly listed in Table 6. It is seen that Reynolds numbers are of the same order of magnitude. Also, except for one study, the rest of the works are performed in water medium. The robustness of the turbulent wake in water compared to air causes buffeting to be mostly effective to be used in energy extraction from the water currents. Furthermore, from the results of Allan and Smith [86] and Armandei and Fernandes [23], it is clear that the efficiency of energy extraction through buffeting is maximized in the vicinity of resonance (Note that for both the frequency ratio is 1). As proved by Gopalkrishnan et al. [85], the propulsive efficiency also is maximized when the structure is in resonance. The reason is because buffeting excitation at resonance will result in an amplitude increase.

3.4. Vortex Induced Vibration (VIV)

A most significant work to harness energy from VIV phenomenon was patented by Bernitsas et al. [91]. Their energy converter is called VIVACE (Vortex Induced Vibration Aquatic Clean Energy) (see Fig. 23) that uses a passive circular cylinder with upward-downward motion, induced by vortex shedding. This passive cylinder is mounted on springs (see Fig. 24) and is exploited to generate electricity in a range of flow velocities. The VIVACE system converts mechanical energy into electricity via rotary or linear generators.

The important parameters that affect the energy extraction by VIV are mass ratio m^*, the mechanical dampingξ, the reduced velocity U^*, the Reynolds number Re and the aspect ratio L/D [94]. To consider the effects of different parameters on VIV performance, Barrero-Gil et al. [94] have performed a parametric study by mathematical modeling on a cylinder with diameter D which has sinusoidal oscillation steadily by amplitude A and frequency *f*. They have formulated the efficiency in terms of the normalized amplitude (A^*=A/D), normalized velocity (U^*=U/(f_ND) and normalized frequency(f^*=f/f_N) as:

$$\eta = \pi A^* C_Y \sin\phi \left(\frac{f^*}{U^*}\right) \tag{21}$$

where $C_Y \sin\phi$is known as the fluid force excitation coefficient that C_Y is drag coefficient in the direction of cylinder motion and Φ is the phase angle by which the fluid force leads the cylinder displacement.

Lee and Bernitsas [95] concluded by experiments that the damping has a strong influence in the maximum efficiency attainable. The mass ratio affects the amplitude of oscillation as depicted in Fig. 7. Therefore, achievable efficiency is affected by the product of m^* and ζ, i.e. mass-damping ratio ($m^*\zeta$). Fig. 25 depicts the dependency of efficiency to mass-damping ratio. It can be inferred from Fig. 25 that a low mass ratio leads to widen the flow velocity range of significant efficiency and an appropriate damping leads to get a high value of maximum efficiency [94]. Therefore, maximum efficiency achieves at the optimum mass-damping ratio.

Transverse galloping is the most useful phenomenon in expanding the range of flow velocity for energy harnessing. VIV occurs within a closed velocity range while transverse galloping exists above certain flow velocity typically after the VIV range [96]. The initiation of transverse galloping does not depend on K (spring stiffness) but only on the absolute flow velocity and also geometric and dynamic characteristics of the oscillator. Higher damping would require a higher velocity to initiate transverse galloping.

MRELAB [97] has proposed a creative method to enhance the power harnessing from VIV of circular cylinder, i.e. PTC (Passive turbulence control). The PTC is in the form of selectively distributed surface roughness for circular cylinder which provides transverse galloping phenomenon after VIV upper branch. Referring to Fig. 26, the amplitude of oscillation in transverse galloping range increases up to 3 diameters while, in synchronization range this value is 1.65 D [97]. The frequency of oscillation (see Fig. 27) decreases slightly where transvers galloping happens. According to Eq. (21), any increase in amplitude causes an increase in efficiency whereas any reduction in f* results in efficiency decrement. Inasmuch as the reduction of f* in comparison with increasing of A* in transverse galloping is negligible, consequently, by transverse galloping more energy is harvested in higher Reynolds number.

Thus MRELAB built a nonlinear oscillator which initiates at low velocities with VIV and continues with transverse galloping which ends only with the destruction of the oscillator as velocity increases. The PTC makes the VIVACE Converter operate at a very broad range of synchronization and therefore broad range of velocities. In Table 7, a brief review is given for energy harvesting by VIV phenomenon.

Different cross sections were studied by researchers that have been listed in Table 7. Particular shape of Q-trapazoid shows the highest efficiency whereas the triangle cross section gives low efficiency value. Based on the studies, achieving to the higher efficiency is possible by decreasing the mass-damping ratio ($m^*\zeta$). Consequently, by decreasing the $m^*\xi$, the maximum value of A* and f* increase, as well.

3.5. Autorotation

One of the turbines that uses Autorotation phenomenon as the principle of operation is VAACT (Vertical Axis Autorotation Current Turbine) which was introduced by Rostami-Fernandes in 2013 with blade shape of flat plate [99]. This turbine composes an extra mass moment of inertia to enhance its operational characteristics such as improvement of the impulsive rotation of the flat plate in the current to regular continuous rotation, and also the performance of turbine [99]. This turbine has two different configurations based on the blade shape as flat plate type and flapped plate type (S shape type) (see Fig. 28). This turbine is deployed in very low speed current (less than 0.4 m/s).Continuous rotation in the VAACT demands these two conditions

Table 10
Definition of swept area and swept volume for each phenomenon.

Phenomenon	Scheme	Swept Area	Swept Volume
Flutter	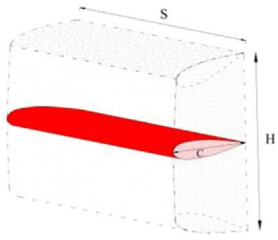	$2.55C^{*}S$ (H=2.55C)[63]	$2.55C^{2}{*}S$
Torsional Galloping	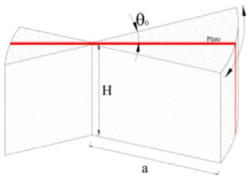	$2\theta_0 Ha$	$2\theta_0 H[a^2-(C-a)^2]$
Buffeting	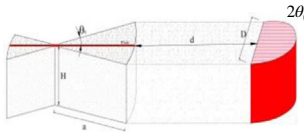	$2\theta_0 Ha$	$2\theta_0 H[a^2-(C-a)^2]+d{*}D{*}H+\frac{\pi}{2}H\left(\frac{D}{2}\right)^2$
Vortex Induced Vibration (VIV) and Transverse Galloping	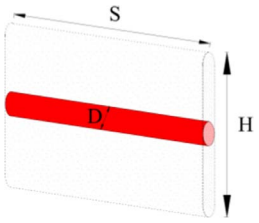	$H{*}S$	$H{*}S{*}D$
Autorotation	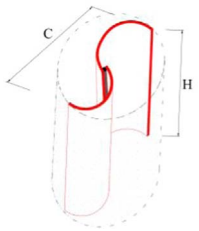	$H{*}C$	$\frac{\pi}{4}HC^2$

simultaneously; the appropriate initial exciting moment and the large enough mass moment of inertia. The first condition refers to an adequate starting moment to stir up the plate from rest, and the second condition to a sufficient moment to keep the full rotational motion. The starting moment is provided by a preliminary angle of attack that the plate is released from because exciting torque is applied by the hydrodynamic forces (Lift and drag force). Main part of the exciting torque in low angle of attacks is provided by the lift force wherein the lift force is dominant (see Fig. 29-A) whereas, in high angle of attacks, the drag force gives the torque to the plate (see Fig. 29-B). Then this turbine is Lift-drag type.

Savonius rotor is another type of autorotated turbine with comparatively low operating speeds in optimum point of performance and can run successfully in the regions where water speed is around 0.4–1 m/s (wind speed is around 4–10 m/s) [100]. Although this turbine originally composes two simple circular-shaped buckets which resem-

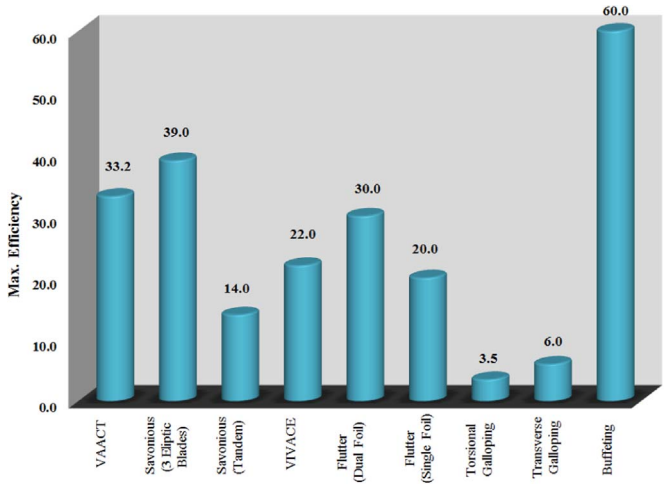

Fig. 31. Maximum achievable efficiency corresponding to various hydrokinetic turbines.

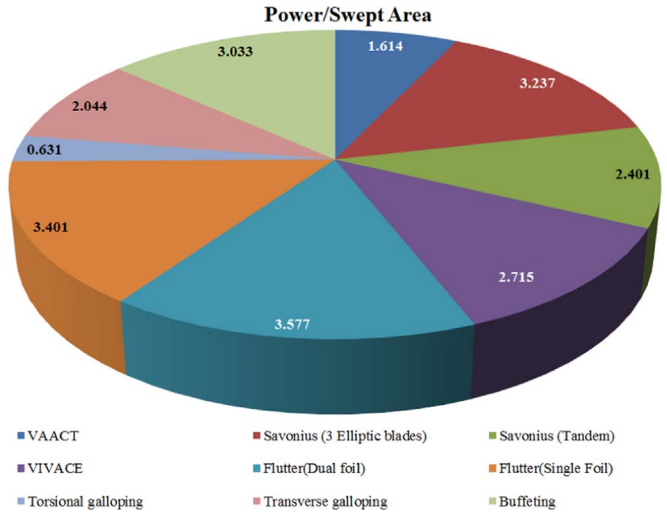

Fig. 32. Power per swept area for different hydrokinetic turbines.

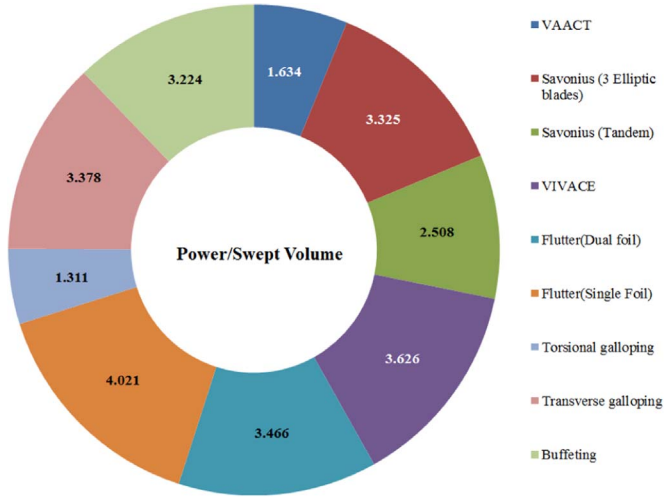

Fig. 33. Power per swept volume of hydrokinetic turbines.

bles the cross section of the letter 'S', in developed configuration the researchers proposed three buckets with modified circular shape. Besides good starting characteristics, Savonius known as omnidirectional turbine which is capable to operate in the current from any direction.

Table 11
Definition of parameters and their values that are used for calculation LCOE in Eq. (22).

Item	Given Value
ICC (installed capital cost in $/kW)	Listed inTable 12
AOE (after-tax annual operating expenses in $/kW-yr)	*LLC* + O & M + *LRC*
AEP_{net} (net annual energy production in MWh/MW/yr)	Capacity in $MW \times 8760 \times CF_{net}$
FCR is the fixed charge rate in %	$\frac{d(1+d)^n}{(1+d)^n-1} \times \frac{1-(T \times PVdep)}{(1-T)}$
d (discount rate in %)	8
n(operational life in years)	20
T (effective tax rate in %)	38.9
PVdep (present value of depreciation in %)	0
CFnet(net capacity factor in %)	0.9
LLC (land lease cost in $/kW-yr)	0
O & M (after-tax levelized operation and maintenance in %)	3
LRC (levelized replacement cost in $/kW-yr)	0
Capacity (MW)	10

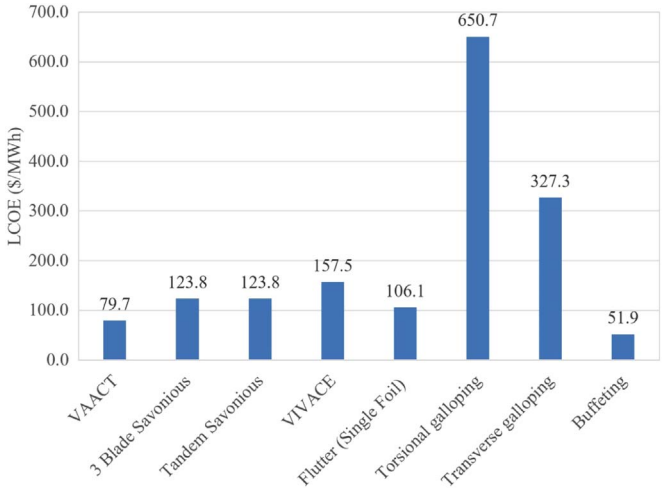

Fig. 34. LCOE (in $/MWh) of the flow-induced motion based prototypes.

Table 12
The value of ICC which is used in Eq. (22).

	ICC ($/kW)
Flutter (Single Foil)	3000.0[113]
VIVACE	4451.5[114]
Savonius	3500.0[115]
Buffeting	1468.4 (calculated by authors)
Torsional Galloping	18,396.0 (calculated by authors)
Transverse Galloping	9253.1 (calculated by authors)
VAACT	2252.6 (calculated by authors)

Savonius rotor is not a pure drag machine. As shown in Fig. 30, however, at every angle of attack except in the range of 115–140, the drag force is greater than the lift force; therefore the drag force of the blade is the main driving force which contributes to the torque production. Due to the high starting torque, Savonius turbine is used for starting of other types of turbine that have lower starting torques, e.g. Darrius turbine [101]. Wind tunnel studies reveal that Savonius turbine with twisted blades is better in terms of smooth running, higher efficiency and self-starting capability in comparison with the semicircular bladed rotor.

In Table 8, a literature review on the Autorotation based turbines is given. In spite of the massive works conducted for autorotating

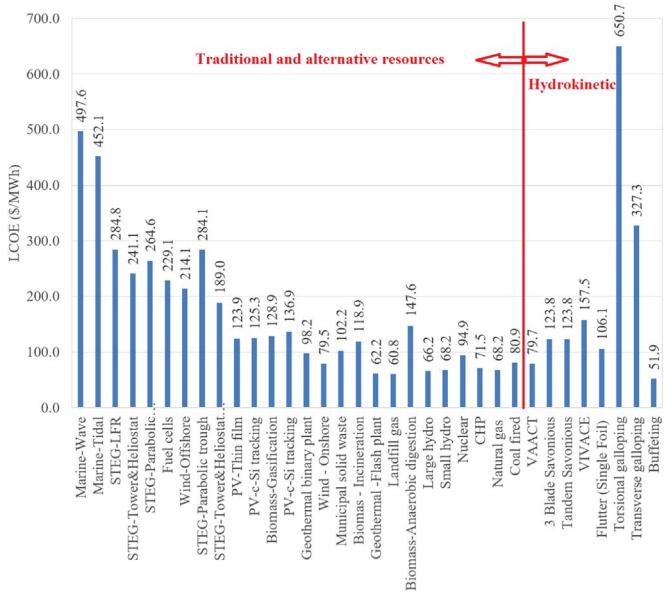

Fig. 35. LCOE of the hydrokinetic resource (vortex-induced motion based technologies) together with the other traditional and alternative renewable energy resources [116].

turbines, the authors have referred to works in Table 8 because of their fame and citations in this field.

4. Benchmarking

In this section, the energy harvesting capability of the turbines based on each phenomenon discussed above is benchmarked. To analyze the capability of VIM based turbines in energy generation, from each VIM phenomenon type the turbine which has the maximum efficiency was chosen. The chosen turbines are listed in Table 9. In this table, swept area is defined as the maximum area used by turbine for power generation whereas swept volume is the effective volume of each turbine which participates in energy harvesting. The scheme of swept volume and swept area of each turbine is given in Table 10.

In the last column of Table 9, annual power generation is calculated for each turbine. However, the rate of power generation is not the only parameter to assess turbine capability. Based on the definition of hydrokinetic turbines for harvesting energy from the current, the cut-in velocity is an important parameter. Some of the turbines mentioned in Table 9 require high cut-in velocity for operation whereas such high velocities are found in limited rivers and ocean currents around the world. As an example Flutter type turbines, in spite of high energy generation, operate in high current velocity.

The maximum achievable efficiencies of the turbines listed in Table 9 are depicted in Fig. 31. As can be seen, among all, the Buffeting turbine can extract energy from low head current with the highest efficiency of 60% and the Torsional Galloping based one has the lowest efficiency of 3.5%. In spite of the low efficiency of the Transverse Galloping based turbine in comparison with others, the phenomenon of Transverse Galloping helps to improve the quality of other phenomena when accompanied by others. For instance, its combination with VIV phenomena in VIVACE has capability to increase the efficiency of energy generation by increasing the amplitude and decreasing the frequency of oscillation [97].

Power per swept area, given in Fig. 32 for each turbine, is defined as the ratio of generated power to maximum perpendicular area to the current that turbine sweeps to generate the corresponding power. The other criterion to benchmark the turbines is the power per swept volume, which is presented in Fig. 33. These parameters give a sense about the size of turbine and its relation to its energy generation. The importance of such parameters is understood when the turbine needs to be installed in bounded fields in depth and width like channels, rivers, etc. The information given in Figs. 32 and 33 is especially important when a farm of turbines is going to be constructed by particular technology in a given space. Based on such criteria for each technology, the number of turbines and total generated power by the farm can be estimated. Furthermore, having the capacity of the farm, these criteria help to indicate the number of required turbines and also area occupied by them. Albeit, the other parameters such as effective distance between turbines in the farm affect the number of turbines in a given space.

Because of high amount of discrepancy between highest and lowest value of the parameters, Figs. 32 and 33 are presented in logarithmic scale to provide the data into same order of magnitude. The highest value of these parameters corresponds to flutter turbine and the lowest one is for torsional galloping based turbine. Therefore, it can be inferred from Figs. 32 and 33 that for arranging a farm of turbines with different technologies in a given space, the flutter based turbine is more appropriate than the others while the Torsional Galloping based turbine is taken into account as an inappropriate technology.

LCOE (Levelized Cost Of Energy) is another benchmarking method, which serves to evaluate the cost of electricity generation of the VIM based turbine prototypes. In simple terms, LCOE is the ratio of present value of total costs to lifetime energy production, and is used to evaluate the relative costs of energy-generating projects and the impact of technology design changes. Different methodologies have been developed to calculate LCOE; the one used for this analysis is fully described in [112]. The following equation is used to calculate LCOE:

$$LCOE = \frac{(ICC \times FCR) + AOE}{(AEP_{net}/1000)} \quad (22)$$

The description of the parameters and their assumed values/formulae are summarized in Table 11. Some parameters, such as present value of depreciation, land lease and levelized replacement costs are not taken into account here. Fig. 34 shows the LCOE (in $/MW h) for the phenomena described in the previous sections. One can observe that among all the prototypes, the energy production via Galloping prototypes (both Transverse and Torsional) costs the most. The majority part of this cost corresponds to construction and installation of technology which is high for the Galloping based turbines. In Galloping based turbine, due to oscillation of the moving parts of the turbine, the risk of fatigue will increase on the structure and therefore, the cost of construction is arisen while the quantity of the generated energy is low. On the other side, the Buffeting and VAACT prototypes cost the least to produce energy. Despite the Buffeting based turbine being of oscillation type and consequently having a high construction cost, the quantity of the energy generation is considerable because of its high efficiency and eventually causes the LCOE to become low. The cost of energy production via other prototypes is in the range of 100–200 $/MW h. Although the principle of VAACT and Savonious type turbines is the same (both are Autorotation), the construction value of Savonious is higher than VAACT due to more complex geometry. As a result, the LOCE of Savonious type turbine is higher than VAACT (Table 12).

In order to have a comparison, LCOE of the hydrokinetic energy extraction via vortex-induced motion based technologies together with the other traditional and alternative energy resources are shown in Fig. 35. The data for the other energy resources is for 2013, taken from Bloomberg New Energy Finance [116]. It can be observed from Fig. 35, among the other types of renewable energy technologies, the Marine Wave and the Marine Tidal are interpreted as much expensive energy conversion methods. It can be justified by the harsh conditions in sea which increases the value of installation and also maintenance besides the high value of construction for Wave Energy Converters (WEC) and Tidal Energy Converters (TEC). However, it can be seen that the highest and lowest LCOE even among the all sources of energy are for the Torsional Galloping and Buffeting prototypes, respectively.

According to Fig. 35, the price of energy generation using hydropower technologies and onshore wind technologies shows a similar order of magnitude with a little discrepancy and the price of these technologies is decreasing every day. The reason is referred to huge volume of research which are being done in the world in order to find new technologies for exploiting these sources as efficient as possible.

5. Conclusion

This paper was devoted to review the technologies for energy harvesting using vortex-induced motions. Each vortex consists of energy when separates from body and sheds into the fluid current. Hence, the vortex causes a motion in the body from which it is separated or in the object which comes in downstream. Such a motion has great potential to harvest energy. In this paper, the whole vortex-induced motion phenomena were classified into several groups which include Flutter, Transverse and Torsional Galloping, Buffeting, Vortex Induced Vibration (VIV), and Fluttering-Autorotation. Then, existing technologies for energy extraction based on the VIM phenomena were reviewed. These technologies were benchmarked for energy harvesting by VIM by the maximum achievable efficiency of different turbine, the criterion of power per swept area, and the criterion of power per swept volume. To do the benchmarking of VIM based energy generation technologies, from each VIM phenomenon type the turbine with the maximum efficiency was chosen. Finally, evidence was given for the cost of hydrokinetic energy conversion using VIM technologies by comparing their cost of energy generation with the cost of other energy resources. This comparison reveals that some kinds of VIM technologies such as Buffeting produce energy with the low cost whereas other kinds such as Torsional Galloping are expensive for being energy convertor.

Acknowledgement

The authors would like to acknowledge gratefully CNPq (Conselho Nacional da Pequisa) for the funding of this research.

References

[1] Peng Z, Zhu Q. Energy harvesting through flow-induced oscillations of a foil. Phys Fluids (1994-Present) 2009;21(12):123602.
[2] Lamb H. Hydrodynamics, 6th edition. NY,USA: Dover Publication; 1945.
[3] Salehi M, Ghadimi P, Rostami AB. A more robust multiparameter conformal mapping method for geometry generation of any arbitrary ship section. J Eng Math 2014;89(1):113–36.
[4] Van Oudheusden, B.W. Investigation of an Aeroelastic Oscillator: Analysis of One-Degree-of-Freedom Galloping with Combined Translational and Torsional Effects". Delft University of Technology, Faculty of Aerospace Engineering, Report LR-707; 1992
[5] Ghadimi P, Bandari HP, Rostami AB. Determination of the heave and pitch motions of a floating cylinder by analytical solution of its diffraction problem and examination of the effects of geometric parameters on its dynamics in regular waves. Int J Appl Math Res 2012;1(4):611–33.
[6] Jung HJ, Lee SW. The experimental validation of a new energy harvesting system based on the wake galloping phenomenon. Smart Mater Struct 2011;20(5):055022.
[7] Ghadimi P, Rostami AB, Jafarkazemi F. Aerodynamic analysis of the boundary layer region of symmetric airfoils at ground proximity. Aerosp Sci Technol 2012;17(1):7–20.
[8] Wardlaw RL. Flutter and torsional instability. Vienna: Springer; 1994. p. 293–319.
[9] Singh K, Michelin S, De Langre E. Energy harvesting from axial fluid-elastic instabilities of a cylinder. J Fluids Struct 2012;30:159–72.
[10] Fei, F., Li, W. J. (2009, December). A fluttering-to-electrical energy transduction system for consumer electronics applications. In: Proceedings of the 2009 IEEE International Conference on Robotics and Biomimetics (ROBIO) pp. 580–585.
[11] Librescu L, Marzocca P. Advances in the linear/nonlinear control of aeroelastic structural systems. Acta Mech 2005;178(3–4):147–86.
[12] Kollmann, W., Umont, G. (2004, December). Lamb vector properties of swirling jets. In: Proceedings of the Fifteenth Australasian fluid mechanics conference, Sydney, Australia pp. 13–17.
[13] Païdoussis MP, Price SJ, de Langre E. Fluid-structure interactions: cross-flow-induced Instabilities. NY, USA: Cambridge University Press; 2011.
[14] Blevins RD. Flow induced vibration, 2nd ed.. FL,USA: Krieger Publication Company; 1994.
[15] Jung HJ, Lee SW. The experimental validation of a new energy harvesting system based on the wake galloping phenomenon. Smart Mater Struct 2011;20(5):055022.
[16] Van Oudheusden BW. On the quasi-steady analysis of one-degree-of-freedom galloping with combined translational and rotational effects. Nonlinear Dyn 1995;8(4):435–51.
[17] Alonso G, Meseguer J, Pérez-Grande I. Galloping instabilities of two-dimensional triangular cross-section bodies. Exp Fluids 2005;38(6):789–95.
[18] Billah K, Scanlan R. Resonance, Tacoma narrows bridge failure, and undergraduate physics textbooks. Am J Phys 1990;59(2):118–24.
[19] Fernandes AC, Armandei M. Low-head hydropower extraction based on torsional galloping. Renew Energy 2014;69:447–52.
[20] Ahmadi G. Aeroelastic wind energy converter. J Energy Convers 1978;18(2):115–20.
[21] Fernandes AC, Armandei M. Phenomenological model for torsional galloping of an elastic flat plate due to hydrodynamic loads. J Hydrodyn Ser B 2014;26:57–65.
[22] Armandei M, Fernandes A. Torsional instability of an elastic flat plate due to hydrodynamic loads. J Mech 2014;30(06):643–50.
[23] Armandei M, Fernandes A. Marine current energy extraction through buffeting. Int J Mar Energy 2016;14:52–67.
[24] Armandei M, Fernandes AC, Bakhshandeh Rostami A. Hydroelastic buffeting assessment over a vertically hinged flat plate. Exp Tech 2016;40:833–9.
[25] Naudascher E, Rockwell D. Flow-induced vibrations: an engineering guide. Corrected edition. Mineola: Dover Publications; 2005.
[26] Jadic I, So RMC, Mignolet MP. Analysis of fluid-structure interactions using a time marching technique. J Fluids Struct 1998;12:631–54.
[27] Caruana D, Despré C, Mignosi A, Corrège M, Le Pourhiet A.. BST and buffeting active control with a flap actuator.InInstrumentation in Aerospace Simulation Facilities, 2001. In: Proceedings of the IEEE 19th International Congress on ICIASF 2001 (pp. 386–396); 2001.
[28] Connor RJ. Fatigue Loading and Design Methodology for High-Mast Lighting Towers. NCHRP (National Corporative Highway Research Program), report 718; 2012.
[29] Liao JC, Beal DN, Lauder GV, Triantafyllou MS. Fish exploiting vortices decrease muscle activity. Science 2003;302:1566–9.
[30] Beal DN, Hover FS, Triantafyllou MS, Liao JC, Lauder GV. Passive propulsion in vortex wakes. J Fluid Mech 2006;549:385–402.
[31] Koumoutsakos P, Leonard A. High-resolution simulations of the flow around an impulsively started cylinder using vortex methods. J Fluid Mech 1995;296:1–38.
[32] Williamson CHK, Govardhan R. A brief review of recent results in vortex-induced vibrations. J Wind Eng Ind Aerodyn 2008;96(6):713–35.
[33] Fernandes, A. C., Rostami, A. B., Canzian, L. G., Sefat, S. M. Vertical axis current turbine (VACT) and its efficiency. In: ASME 2013 Proceedings of the 32nd International Conference on Ocean, Offshore and Arctic Engineering (pp. V008T09A051-V008T09A051). American Society of Mechanical Engineers; 2013.
[34] Rostami, A. B., Fernandes, A. C. Plate Shape Effect on the Performance of the Vertical Axis Auto Rotation Current Turbine (VAACT). In: ASME 2014 Proceedings of the 33rd International Conference on Ocean, Offshore and Arctic Engineering (pp. V09AT09A041-V09AT09A041). American Society of Mechanical Engineers; 2014.
[35] Iversen JD. Autorotating flat-plate wings: the effect of the moment of inertia, geometry and Reynolds number. J Fluid Mech 1979;92(02):327–48.
[36] Lugt HJ. Autorotation. Annu Rev Fluid Mech 1983;15(1):123–47.
[37] Riabouchinsky DP. Thirty years of theoretical and experimental research in fluid mechanics. J R Aeronaut Soc 1935;39(282–348):377–444.
[38] Skew BW. Autorotation of many sided bodies in an airstream. Nature 1991;352:512–3.
[39] Bakhshandeh Rostami A. Hydrokinetic energy harvesting by autorotation of a plate with hinged axis [PhD Thesis]. Brazil: Federal University of Rio de Janeiro; 2015.
[40] Bakhshandeh rostamiA., FernandesA.C. Simulation of Fluttering and Autorotation motion of Vertically Hinged Flat Plate. In: Proceedings of the ASME 2015 34nd International Conference on Ocean, Offshore and Arctic Engineering St. John´s, NL, Canada: OMAE2015-41244.
[41] Field SB, Klaus M, Moore MG, Nori F. Chaotic dynamics of falling disks. Nature 1997;388(6639):252–4.
[42] Belmonte A, Eisenberg H, Moses E. From flutter to tumble: inertial drag and Froude similarity in falling paper. Phys Rev Lett 1998;81(2):345–8.
[43] Willmarth WW, Hawk NE, Harvey RL. Steady and unsteady motions and wakes of freely falling disks. Phys Fluids 1964;7(2):197–208.
[44] Smith EH. Autorotating wings: an experimental investigation. J Fluid Mech 1971;50(03):513–34.
[45] Andersen A, Pesavento U, Wang ZJ. Unsteady aerodynamics of fluttering and tumbling plates. J Fluid Mech 2005;541:65–90.
[46] Mirzaeisefat S, Fernandes AC. Stability analysis of the fluttering and autorotation of flow-induced rotation of a hinged flat plate. J Hydrodyn Ser B 2013;25(5):755–62.
[47] Mittal R, Seshadri V, Udaykumar HS. Flutter, tumble and vortex induced autorotation. J Theor Comput Fluid Dyn 2004;17:165–70.
[48] Andersen A, Pesavento U, Wang Z. Analysis of transitions between fluttering, tumbling and steady descent of falling cards. J Fluid Mech 2005;541:91–104.
[49] Andronov PR, Grigorenko DA, Guvernyuk SV, Dynnikova GY. Numerical simulation of plate autorotation in a viscous fluid flow. J Fluid Dyn 2007;42–5:719–31.
[50] Lugt HJ. Autorotation of an elliptic cylinder about an axis perpendicular to the flow. J Fluid Mech 1980;99(4):817–40.
[51] Wu RJ, Lin S-Y. The flow of a falling ellipse: numerical method and classification.

J Mech 2015;31:771–82.
[52] Siala F, Liburdy JA. Energy harvesting of a heaving and forward pitching wing with a passively actuated trailing edge. J Fluids Struct 2015;57:1–14.
[53] Xiao Q, Zhu Q. A review on flow energy harvesters based on flapping foils. J Fluids Struct 2014;46:174–91.
[54] Young J, Lai JC, Platzer MF. A review of progress and challenges in flapping foil power generation. Prog Aerosp Sci 2014;67:2–28.
[55] Ashraf MA, Young J, Lai JCS, Platzer MF. Numerical analysis of an oscillating-wing wind and hydropower generator. AIAA J 2011;49(7):1374–86.
[56] Abiru H, Yoshitake A. Study on a flapping wing hydroelectric power generation system. J Environ Eng 2011;6:178–86.
[57] Huxham, G., Cochard, S., Patterson, J., 2012. Experimental parametric investigation of an oscillating hydrofoil tidal stream energy converter. In: Proceedings of the 18th Australasian Fluid Mechanics Conference AFMC 2012. Australasian Fluid Mechanics Society, Launceston, Tasmania.
[58] SimpsonB.J., Hover, F.S., Triantafyllou, M.S., 2008a. Experiments in direct energy extraction through flapping foils. In: Proceedings of the Eighteenth International Offshore and Polar Engineering Conference. July 6–11, 2008, Canada.
[59] Platzer M, Ashraf M, Young J, Lai J. Extracting power in jet streams: pushing the performance of flapping wing technology. In: Proceedings of the 27th Congress of the International Council of the Aeronautical Sciences. International Council of the Aeronautical Sciences Paper 2010-2.9.1. September 19–24, 2010, Nice, France; 2010.
[60] Usoh, C.O., Young, J., Lai, J.C.S., Ashraf, M.A., Numerical analysis of a non-profiled plate for flapping wing turbines. In: Proceedings of the 18th Australasian Fluid Mechanics Conference, Launceston, Australia; 2012.
[61] Xiao Q, Liao W, Yang SC, Peng Y. How motion trajectory affects energy extraction performance of a biomimic energy generator with an oscillating foil?. Renew Energy 2012;37:61–75.
[62] Hoke CM, Young J, Lai JCS. Effects of time-varying camber deformation on flapping foil propulsion and power extraction. J Fluids Struct 2015;56:152–76.
[63] Kinsey T, Dumas G, Lalande G, Ruel J, Mehut A, Viarouge P, Jean Y. Prototype testing of a hydrokinetic turbine based on oscillating hydrofoils. Renew Energy 2011;36(6):1710–8.
[64] The Engineering Business Ltd. Stingray Tidal Stream Energy Device – Phase 1. Technical Report; 2002.
[65] The Engineering Business Ltd. Stingray Tidal Stream Energy Device – Phase 2. Technical Report; 2003.
[66] The Engineering Business Ltd. Stingray Tidal Stream Energy Device – Phase 3. Technical Report; 2005.
[67] Pulse Tidal Limited. ⟨http://www.pulsetidal.com⟩. [Visited at 28 January]; 2016.
[68] BioPower Systems. ⟨http://www.biopowersystems.com⟩. [Visited at 27 September]; 2016.
[69] http://www.maritimejournal.com/news101/marine-renewable energy/funding_flow_for_shallow_water_tidal_stream_power_generator. [Visited at 27 June, 2016]
[70] BBC report on PulseTidal prototype. ⟨https://www.youtube.com/watch?V=z07OV0d9NS4⟩. [Visited at 27 September]; 2016.
[71] Aniprop, ⟨http://www.aniprop.de/dlrhp⟩ [accessed at 25 September 2016].
[72] Send W, Scharstein F, Scharstein H. German Patent DPMA 101 09 475. IPC F03B 13/00 (2006.01); 2010.
[73] Festo automation technology company, ⟨https://www.festo.com/group/en/cms/10222.htm⟩. [accessed at 27 September 2016]
[74] DualWingGenerator catalogue, https://www.festo.com/net/SupportPortal/Files/333988/Festo_DualWingGenerator_en.pdf. [accessed at 27 September 2016]
[75] Barrero-Gil A, Alonso G, Sanz-Andres A. Energy harvesting from transverse galloping. J Sound Vib 2010;329(14):2873–83.
[76] Sirohi J, Mahadik R, Piezoelectric wind energy harvester for low-power sensors, Journal of Intelligent Material Systems and Structures, Vol 22 (18) 2215–2228.
[77] Vicente-Ludlam D, Barrero-Gil A, Velazquez A. Optimal electromagnetic energy extraction from transverse galloping. J Fluids Struct 2014;51:281–91.
[78] Vicente-Ludlam D, Barrero-Gil A, Velazquez A. Enhanced mechanical energy extraction from transverse galloping using a dual mass system. J Sound Vib 2015;339:290–303.
[79] Ewere F, Wang G,Performance of galloping piezoelectric energy harvesters, Journal of Intelligent Material Systems and Structures 0(0) 1–12.
[80] Liya Zhao, Lihua Tang, Yaowen Yang. Small Wind Energy Harvesting From Galloping Using Piezoelectric Materials. In: Proceedings of the ASME 2012 Conference on Smart Materials, Adaptive Structures and Intelligent Systems SMASIS2012 September 19-21, Stone Mountain, Georgia, USA; 2012.
[81] Dai HL, Abdelkefi A, Javed U, Wang L. Modeling and performance of electromagnetic energy harvesting from galloping oscillations. Smart Mater Struct 2015;24(4):045012.
[82] Ewere F, Wang G, Cain B. Experimental investigation of galloping piezoelectric energy harvesters with square bluff bodies. Smart Mater Struct 2014;23(10):104012.
[83] Bhattacharya A, Shahajhan SSS. Power extraction from vortex-induced angular oscillations of elliptical cylinder. J Fluids Struct 2016;63:140–54.
[84] Armandei, M., Fernandes, A. C. Performance Improvement and Similarity Analysis for Torsional Galloping Based Turbine. In: Proceedings of the ASME 2015 34th International Conference on Ocean, Offshore and Arctic Engineering(pp. V009T09A014-V009T09A014). American Society of Mechanical Engineers; 2015.
[85] Gopalkrishnan R, Triantafyllou MS, Triantafyllou GS, Barrett D. Active vorticity control in a shear flow using a flapping foil. J Fluid Mech 1994;274:1–21.
[86] Allen JJ, Smits AJ. Energy harvesting Eel [April]. J Fluids Struct 2001;15(Issues 3–4):629–40.
[87] Techet AH, Allen JJ, Smits AJ. Piezoelectric Eels for energy harvesting in the ocean. Kitakyushu, Japan: ISOPE; 2002.
[88] Allen, J.J., Techet, A.H., Kelso, R.M., Smits, A.J., Energy Harvesting Eel, In: Proceedings of the 14th Australasian Fluid Mechanics Conference Adelaide University, Adelaide, Australia 10-14 December 2001.
[89] Taylor GW, Burns JR, Kammann SM, Powers WB, Welsh TR. The energy harvesting Eel: a small subsurface Ocean/River power generator [October]. IEEE J Ocean Eng 2001;26(4), [October].
[90] Wenai Shen , Zhu Songye. Harvesting energy via electromagnetic damper: application to bridge stay cables. J Intell Mater Syst Struct 2015;26(1):3–19.
[91] Bernitsas MM, Raghavan K, Ben-Simon Y, Garcia EM. VIVACE (Vortex Induced Vibration Aquatic Clean Energy): a new concept in generation of clean and renewable energy from fluid flow. J Offshore Mech Arct Eng 2008;130(4):041101.
[92] http://en.openei.org/wiki/MHK_Technologies/Vortex_Induced_Vibrations_Aquatic_Clean_Energy_VIVACE).[Visited at 27 June, 2016]
[93] Bernitsas MM, Ben-Simon Y, Raghavan K, Garcia EM. The VIVACE converter: model tests at high damping and Reynolds number around 105. J Offshore Mech Arct Eng 2009;131(1):011102.
[94] Barrero-Gil A, Pindado S, Avila S. Extracting energy from vortex-induced vibrations: a parametric study. Appl Math Model 2012;36(7):3153–60.
[95] Lee JH, Bernitsas MM. High-damping, high-Reynolds VIV tests for energy harnessing using the VIVACE converter. Ocean Eng 2011;38(16):1697–712.
[96] Park H, Kumar RA, Bernitsas MM. Enhancement of flow-induced motion of rigid circular cylinder on springs by localized surface roughness at 3×10 4≤ Re≤1.2×10 5. Ocean Eng 2013;72:403–15.
[97] Chang CCJ, Kumar RA, Bernitsas MM. VIV and galloping of single circular cylinder with surface roughness at 3.0×10 4≤ Re≤1.2×10 5. Ocean Eng 2011;38(16):1713–32.
[98] Ding L, Zhang L, Wu C, Mao X, Jiang D. Flow induced motion and energy harvesting of bluff bodies with different cross sections. Energy Convers Manag 2015;91:416–26.
[99] Fernandes AC, Rostami AB, Canzian LG, Sefat SM. June). Vertical axis current turbine (VACT) and its efficiency. In: ASME 2013 Proceedings of the 32nd International Conference on Ocean, Offshore and Arctic Engineering (pp. V008T09A051-V008T09A051). American Society of Mechanical Engineers; 2013.
[100] Roy S, Saha UK. Review of experimental investigations into the design, performance and optimization of the Savonius rotor. In: Proceedings of the Institution of Mechanical Engineers, Part A: Journal of Power and Energy, 227(4), 528-542; 2013.
[101] Kamoji MA, Kedare SB, Prabhu SV. Experimental investigations on single stage modified Savonius rotor. Appl Energy 2009;86(7):1064–73.
[102] Kyozuka Y. An experimental study on the Darrieus-Savonius turbine for the tidal current power generation. J Fluid Sci Technol 2008;3(3):439–49.
[103] Sarma NK, Biswas A, Misra RD. Experimental and computational evaluation of Savonius hydrokinetic turbine for low velocity condition with comparison to Savonius wind turbine at the same input power. Energy Convers Manag 2014;83:88–98.
[104] Damak A, Driss Z, Abid MS. Experimental investigation of helical Savonius rotor with a twist of 180. Renew Energy 2013;52:136–42.
[105] Kamoji MA, Kedare SB, Prabhu SV. Performance tests on helical Savonius rotors. Renew Energy 2009;34(3):521–9.
[106] Saha UK, Rajkumar MJ. On the performance analysis of Savonius rotor with twisted blades. Renew Energy 2006;31(11):1776–88.
[107] Dobrev I, Massouh F. CFD and PIV investigation of unsteady flow through Savonius wind turbine. Energy Procedia 2011;6:711–20.
[108] Golecha K, Eldho TI, Prabhu SV. Study on the interaction between two hydrokinetic savonius turbines. Int J Rotating Mach 2012:2012.
[109] Golecha K, Eldho TI, Prabhu SV. Influence of the deflector plate on the performance of modified Savonius water turbine. Appl Energy 2011;88(9):3207–17.
[110] Rostami AB, Fernandes AC. The effect of inertia and flap on autorotation applied for hydrokinetic energy harvesting. Appl Energy 2015;143:312–23.
[111] Fernandes AC, Rostami AB. Hydrokinetic energy harvesting by an innovative vertical axis current turbine. Renew Energy 2015;81:694–706.
[112] Short W, Packey DJ, Holt T. A Manual for the Economic Evaluation of Energy Efficiency and Renewable Energy Technologies. Golden, CO, National Renewable Energy Laboratory. March 1995. ⟨http://www.nrel.gov/docs/legosti/old/5173.pdf⟩. Accessed February; 1995.
[113] DTI. "Stingray Tidal Stream Energy Device – Phase 3." Retrieved 02 May 2006, from: ⟨http://www.dti.gov.uk/renewables/publications/pdfs/T00211.pdf⟩; 2005.
[114] Raghavan Kamaldev. Energy extraction from a steady flow using vortex induced vibration [PhD Thesis]. MI,USA: The University of Michigan; 2007.
[115] Smart Turbine Inc. http://www.smart-turbine.com/[accessed at 27 September 2016]
[116] World Energy council. World Energy Perspective: Cost of Energy Technologies. Project partner: Bloomberg New Energy Finance; 2013.